

Physical Oceanography - UNAM, Mexico

Lecture 3: The Wind-Driven Oceanic Circulation

Robin Waldman

September 13th, 2018

Contact :
CNRM, Météo France - CNRS
+33561079336
robin.waldman@meteo.fr

Contents

1	The Ekman currents and Sverdrup balance	3
1.1	Ekman currents	3
1.1.1	Hypotheses and derivation	3
1.1.2	Ekman transports	3
1.1.3	Ekman pumping	4
1.1.4	The Ekman spiral	6
1.2	The Sverdrup balance	7
1.2.1	The barotropic vorticity equation	7
1.2.2	Sverdrup's hypotheses and equation	9
1.2.3	Interpretation in terms of Ekman and geostrophic flow	10
2	The western intensification of gyres	14
2.1	Bottom friction: Stommel model	14
2.2	Lateral friction: Munk model	15
2.3	Topographic torques	16
2.4	Recirculation gyres	19
2.5	Eastern shadow zones	21
3	The Southern Ocean circulation	25
3.1	Meridional overturning: the Deacon Cell	25
3.1.1	Ekman transports	25
3.1.2	Meridional geostrophic response	26
3.1.3	Interpreting the barotropic vorticity equation	27
3.2	Mean zonal circulation	27
3.2.1	Pressure gradient build-up by Ekman transports	28
3.2.2	Zonal interior geostrophic flow	29
3.2.3	What slows down the Antarctic Circumpolar Current?	30
3.3	Role of eddies	30
3.3.1	Eddy-driven meridional heat transport	30
3.3.2	Role of standing meanders	31
3.3.3	Role of transient eddies	32
3.4	An energetic interpretation: the oceanic Lorenz Energy Cycle	34
4	The Tropical circulation	37
4.1	Meridional circulation	37
4.1.1	Tropical gyres	37
4.1.2	Tropical cells	37
4.1.3	Tropical Instability Waves	39
4.1.4	Tropical-subtropical connections: the Subtropical Cells	40
4.2	Zonal circulation	40
4.2.1	South Equatorial Currents	41
4.2.2	North Equatorial Countercurrent	43
4.2.3	Equatorial undercurrent	43

1 The Ekman currents and Sverdrup balance

We have introduced in Chapter 1 both the Ekman currents and the Sverdrup balance, two fundamental theories which interpret the structure of near-surface currents and the existence of gyres in the ocean. The former appeared in Chapter 2 as a leading-order balance near the surface. Both of them illustrate the central role that the atmosphere plays in setting the ocean into motion.

1.1 Ekman currents

1.1.1 Hypotheses and derivation

We have seen in Chapter 1 that the Ekman theory was the first quantitative theory relating the winds and ocean circulation. In Chapter 2, we have deduced the equation for the Ekman currents by applying a dimensional analysis to the horizontal momentum equations. Indeed, we found that near the surface, where vertical turbulent momentum exchanges (modelled as diffusivities) are intense, the momentum balance is driven by the Coriolis acceleration, the pressure forces and vertical turbulent fluxes. The equilibration between Coriolis and pressure forces describes the geostrophic currents, while that between Coriolis and vertical turbulent fluxes describes the Ekman currents. Actually, Ekman originally formulated a stronger set of hypotheses to obtain his wind-driven currents, very similar to those posed to formulate the single-column version of NEMO model. He assumed that:

- The ocean is infinitely large and wide (as in the dimensional analysis and NEMO1D model), so that interactions with topography can be neglected;
- It has reached a steady state (as in the dimensional analysis), so that the Eulerian derivative $\frac{\partial \mathbf{u}_h}{\partial t} = \mathbf{0}$;
- It is homogeneous horizontally (as in the dimensional analysis and NEMO1D model), so that $(\mathbf{u}_h \cdot \nabla) \mathbf{u}_h = 0$, $\nabla_h \cdot (\kappa_{hu} \nabla_h) \mathbf{u}_h = 0$ and by continuity $w = 0$ hence $w \frac{\partial \mathbf{u}_h}{\partial z} = 0$;
- Its density is constant, which has the same consequence as the Boussinesq hypotheses for the horizontal momentum equations;
- The vertical eddy diffusivity κ_{zu} is constant.

Hence we obtain the very simplified momentum equations for the stationary Ekman currents:

$$f \mathbf{k} \times \mathbf{u}_E = \kappa_{zu} \frac{\partial^2 \mathbf{u}_E}{\partial z^2}$$

that is:

$$\begin{aligned} u_E &= \frac{\kappa_{zu}}{f} \frac{\partial^2 v_E}{\partial z^2} \\ v_E &= -\frac{\kappa_{zu}}{f} \frac{\partial^2 u_E}{\partial z^2} \end{aligned}$$

1.1.2 Ekman transports

The simplest and most relevant resolution of the Ekman equations for large-scale oceanography concerns the vertically-integrated Ekman transports within the Ekman layer. At the surface, by

continuity of the turbulent vertical fluxes, and as we saw for NEMO model in Chapter 2, we have:

$$\boldsymbol{\tau} = \rho_0 \kappa_{zu} \left. \frac{\partial \mathbf{u}_h}{\partial z} \right|_0$$

with $\boldsymbol{\tau}$ the surface wind stress. Now contrary to Ekman, we assume that at the bottom of the Ekman layer h_E , vertical turbulent fluxes cancel out: $\boldsymbol{\tau}_b = \kappa_{zu} \left. \frac{\partial \mathbf{u}_h}{\partial z} \right|_{-h_E} = 0$. The vertical integration of the Ekman equations hence yields a trivial solution for the Ekman transport:

$$\begin{aligned} U_E &= \int_{-h_E}^0 u_E dz = \left[\frac{\kappa_{zu}}{f} \frac{\partial v_E}{\partial z} \right]_{-h_E}^0 = + \frac{\tau_y}{\rho_0 f} \\ V_E &= \int_{-h_E}^0 v_E dz = \left[- \frac{\kappa_{zu}}{f} \frac{\partial u_E}{\partial z} \right]_{-h_E}^0 = - \frac{\tau_x}{\rho_0 f} \end{aligned}$$

This is one of the most useful relations in physical oceanography. It predicts that the wind-driven Ekman transports are orthogonal to surface winds, to their right in the Northern Hemisphere and to their left in the Southern Hemisphere. This explains the location of the main upwelling regions, which are either due to offshore Ekman transports at the coast (e.g. the California upwelling system) or to divergent Ekman transports (e.g. the Equatorial upwelling). It also predicts that for a given wind, the Ekman transports will be stronger at low latitudes. This explains the particularly strong meridional heat transport by the ocean at low latitudes, as we saw in Chapter 1. Obviously, at the Equator the Coriolis acceleration cancels out and this relation does not hold anymore.

Exercise: upwelling rate of the California upwelling system. We assume an along-coast Northerly wind of $v_{10m} = -10\text{m/s}$ and that the Ekman theory holds at $L = 100\text{km}$ off the coast. Deduce the Ekman volumic transport T_E at that distance across a section of width $W = 100\text{km}$ and depth $-h_E$, and the average upwelling rate at the basis of the Ekman layer $w(-h_E)$ within this coastal box. We assume $C_D \sim 2 \times 10^{-3}$, $\rho_a \sim 1\text{kg/m}^3$, $\rho_0 \sim 1000\text{kg/m}^3$, $f_0 \sim 10^{-4}\text{s}^{-1}$.

Solution: the Ekman volumic transport is $T_E = U_E W = - \frac{C_D \rho_a v_{10m}^2 W}{\rho_0 f_0} = -0.2\text{Sv}$, and hence by continuity (with no normal flow at the coast) the average upwelling rate at the basis of the Ekman layer is $w(-h_E) = - \frac{T_E}{WL} = +2 \times 10^{-5}\text{m/s} \simeq 2\text{m/day}$. We deduce that any equatorward wind along a North-South coast generates an offshore Ekman transport which drives Ekman upwelling. Although the upwelling magnitude seems modest, due to the strong near-surface stratification, it generates intense cold and fresh anomalies in those regions. It is the case of all Eastern Boundary subtropical regions.

1.1.3 Ekman pumping

Another means by which Ekman transports can generate vertical motion is through the so-called Ekman pumping (upwelling) or suction (downwelling). Indeed, if Ekman transports diverge, they induce by continuity vertical motions at the basis of the Ekman layer. We integrate the continuity equation within the Ekman layer:

$$\begin{aligned} \int_{-h_E}^0 \frac{\partial w_E}{\partial z} dz &= - \int_{-h_E}^0 \left(\frac{\partial u_E}{\partial x} + \frac{\partial v_E}{\partial y} \right) dz \\ \implies 0 - w_E(-h_E) &= - \int_{-h_E}^0 \left[\frac{\partial}{\partial x} \left(\frac{\kappa_{zu}}{f} \frac{\partial^2 v_E}{\partial z^2} \right) - \frac{\partial}{\partial y} \left(\frac{\kappa_{zu}}{f} \frac{\partial^2 u_E}{\partial z^2} \right) \right] dz \\ \implies w_E(-h_E) &= \left[\frac{\partial}{\partial x} \left(\frac{\kappa_{zu}}{f} \frac{\partial v_E}{\partial z} \right) - \frac{\partial}{\partial y} \left(\frac{\kappa_{zu}}{f} \frac{\partial u_E}{\partial z} \right) \right]_{-h_E}^0 \\ &= \frac{1}{\rho_0} \left[\frac{\partial}{\partial x} \left(\frac{\tau_y}{f} \right) - \frac{\partial}{\partial y} \left(\frac{\tau_x}{f} \right) \right] \\ &= \frac{\text{Curl}(\boldsymbol{\tau}/f)}{\rho_0} \end{aligned}$$

with $Curl(\mathbf{a}) = [\nabla \times \mathbf{a}]_z$ the vertical vorticity operator. Indeed, because Ekman transports are orthogonal to surface winds, any positive (negative) vorticity of those winds induces a divergence (convergence) of Ekman transports, which by continuity causes upwelling (downwelling) at the basis of the Ekman layer (Fig.1.1). Note that the beta effect can potentially also generate vertical motions even for constant winds, but except at the planetary scale and near the Equator it has a minor role. This explains the deep thermocline at subtropical latitudes between the tropical Easterlies and the mid-latitude Westerlies (negative vorticity of winds hence downwelling) and the shallow one at subpolar latitudes where Westerlies weaken (positive vorticity hence upwelling).

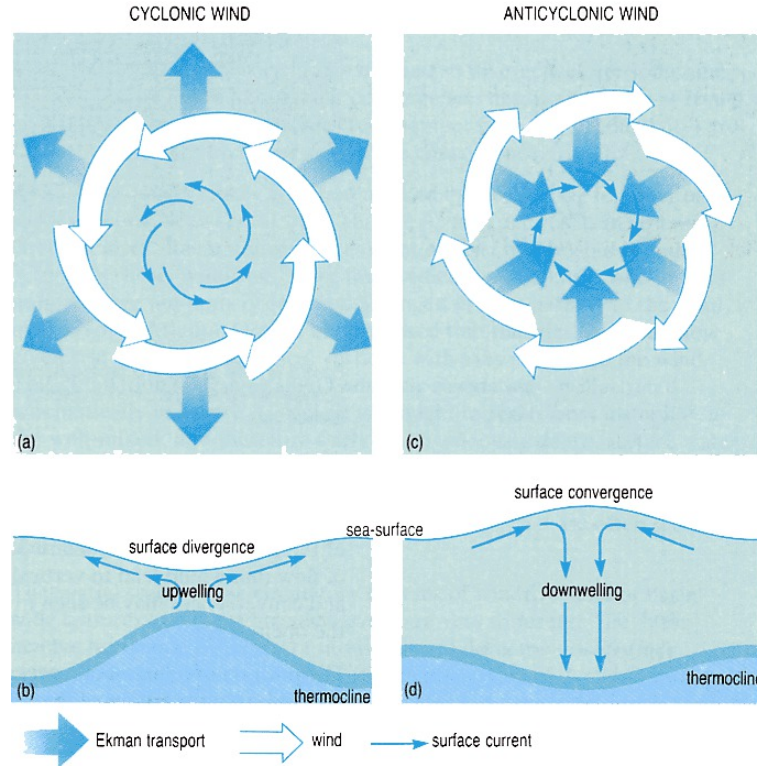


Figure 1.1: Ekman pumping/suction in the Northern Hemisphere.

Exercise: average upwelling rate in the subtropical North Atlantic. We assume that the Easterly wind blows at $u_{10m} = -5m/s$ at $\phi_1 = 10^\circ N$ and that the Westerly wind blows at $u_{20m} = +10m/s$ at $\phi_2 = 40^\circ N$. Deduce the average downwelling rate $w_E(-h_E)$ between those latitudes. We assume $C_D \sim 2 \times 10^{-3}$, $\rho_a \sim 1kg/m^3$, $\rho_0 \sim 1000kg/m^3$, $f_1 \sim 2 \times 10^{-5}s^{-1}$, $f_2 \sim 10^{-4}s^{-1}$, $\Delta y = 3000km$.

Solution: $w_E(-h_E) = \frac{1}{\rho_0} \frac{-\partial \tau_x / f}{\partial y} = \frac{C_D \rho_a}{\rho_0 \Delta y} \left(\frac{-u_{20m}^2}{f_2} - \frac{u_{10m}^2}{f_1} \right) \simeq -2 \times 10^{-6} m/s \simeq -1m/5 \text{ days}$. This Ekman suction is one order of magnitude lower than the Ekman pumping estimated in coastal upwelling systems. But at the climatological timescale, it is sufficient to induce the deep subtropical thermocline.

Exercise: average Equatorial upwelling. We assume that the Easterly wind blows at $u_{10m} = -5m/s$ all along the Equatorial band, and that the Ekman relation is valid at $\phi_1 = 5^\circ N$ and $\phi_2 = 5^\circ S$. Deduce the average poleward Ekman transport over a basin of width $W = 6000km$, and the average upwelling rate in the Equatorial band between both latitudes. Here we assume that $f_0 = \pm 10^{-5}s^{-1}$ at 5° of latitude.

Solution: the problem is symmetric at both latitudes with only f_0 changing sign. We have: $T_E(\phi_1) = U_E(\phi_1)W = +\frac{C_D \rho_a u_{10m}^2 W}{\rho_0 f_0} = +20Sv$, hence $T_E(\phi_2) = -20Sv$. We deduce by continuity:

$w(-h_E) = \frac{T_E(\phi_1) - T_E(\phi_2)}{WL} \simeq 6 \times 10^{-6} \text{ m/s} \simeq 1 \text{ m/day}$. This upwelling rate is much larger than what was found for the subtropical gyre. Indeed, as was mentioned earlier, Ekman transports are much more intense in the Tropics because of the reduced value of f_0 . This Equatorial divergence of Ekman transports largely explains the cold and fresh anomaly of the surface Equatorial ocean.

1.1.4 The Ekman spiral

Although of lesser importance for physical oceanography than the vertically-integrated Ekman transports, the oceanic Ekman spiral allows to predict the rotation of Ekman currents with depth and the relation between the wind stress and the Ekman layer depth. We go back to the Ekman equations that we resolve for the complex variable $\bar{v}_E = u_E + iv_E$, which yields:

$$\begin{aligned} \bar{v}_E &= u_E + iv_E \\ &= \frac{\kappa_{zu}}{f} \left(\frac{\partial^2 v_E}{\partial z^2} - i \frac{\partial^2 u_E}{\partial z^2} \right) \\ &= -\frac{\kappa_{zu}}{f} i \frac{\partial^2 \bar{v}_E}{\partial z^2} \end{aligned}$$

that is:

$$\frac{\partial^2 \bar{v}_E}{\partial z^2} = \frac{if}{\kappa_{zu}} \bar{v}_E$$

It can be simplified by using the polar form: $i = e^{i\pi/2} = (e^{i\pi/4})^2 = \left(\frac{1+i}{\sqrt{2}}\right)^2$. Hence:

$$\frac{\partial^2 \bar{v}_E}{\partial z^2} = \left(\frac{1+i}{h_E}\right)^2 \bar{v}_E$$

with $h_E = \sqrt{2\kappa_{zu}/f}$ the Ekman depth. Hence the solution has the form:

$$\bar{v}_E = \alpha \exp((1+i)z/h_E) + \beta \exp(-(1+i)z/h_E),$$

with α et β two complex integration constants. The boundary conditions are:

- bounded velocities at the ocean bottom: $\bar{v}_E < \infty$ when $z \rightarrow -\infty$, hence $\beta = 0$
- surface turbulent fluxes are equal to the wind stress, which we assume constant and zonal:
 $\tau_0 = \tau_x \mathbf{i} = \rho_0 \kappa_{zu} \frac{\partial \mathbf{u}_E}{\partial z}$.

The surface boundary condition yields:

- $\rho_0 \kappa_{zu} \frac{\Re(\alpha) + \Im(\alpha)}{h_E} = 0 \implies \Im(\alpha) = -\Re(\alpha)$,
- $\rho_0 \kappa_{zu} \frac{\Re(\alpha) - \Im(\alpha)}{h_E} = \tau_x \implies \Re(\alpha) = \frac{\tau_x h_E}{2\rho_0 \kappa_{zu}}$,

hence

$$\begin{aligned} \bar{v}_E &= (1-i) \frac{\tau_x h_E}{2\rho_0 \kappa_{zu}} \exp\left((1+i) \frac{z}{h_E}\right) \\ &= \frac{\tau_x h_E}{\sqrt{2}\rho_0 \kappa_{zu}} \exp\left(i\left(\frac{z}{h_E} - \frac{\pi}{4}\right)\right) \exp\left(\frac{z}{h_E}\right) \end{aligned}$$

that is

$$\begin{aligned} u_E &= V_0 \cos\left(\frac{z}{h_E} - \frac{\pi}{4}\right) \exp\left(\frac{z}{h_E}\right) \\ v_E &= V_0 \sin\left(\frac{z}{h_E} - \frac{\pi}{4}\right) \exp\left(\frac{z}{h_E}\right) \end{aligned}$$

with $V_0 = (\tau_x h_E) / (\sqrt{2} \rho_0 \kappa_{zu}) = \tau_x / (\rho_0 \sqrt{\kappa_{zu} f})$.

Several conclusions arise from this derivation. First the Ekman depth corresponds in the Ekman model to the characteristic depth of exponential decay of wind-driven currents. It reaches typically $h_E \simeq \sqrt{2 \times 0.1 / 10^{-4}} \simeq 50m$, which is very shallow compared to the ocean depth. It does not scale directly with the wind stress, although turbulent diffusivities κ_{zu} are driven by it. Also, the Coriolis dependency indicates that Ekman currents penetrate deeper at low latitudes. Surface currents have an angle of $-\frac{\pi}{4}$ to a purely zonal wind at surface. Hence because of the Earth's rotation they are rotated 45° to the right of surface winds in the Northern Hemisphere, with a magnitude of:

$$V_0 = \frac{\rho_a C_D}{\rho \sqrt{\kappa_{zu} f}} \|\mathbf{u}_{10m}\|^2 \sim 0.02 \|\mathbf{u}_{10m}\|$$

that is typically $20cm/s$ for $\|\mathbf{u}_{10m}\| = 10m/s$. Thus they do not explain the most intense surface currents that we observed in Chapter 1. They spiral to the right with depth in the Northern Hemisphere and weaken exponentially (Fig.1.2).

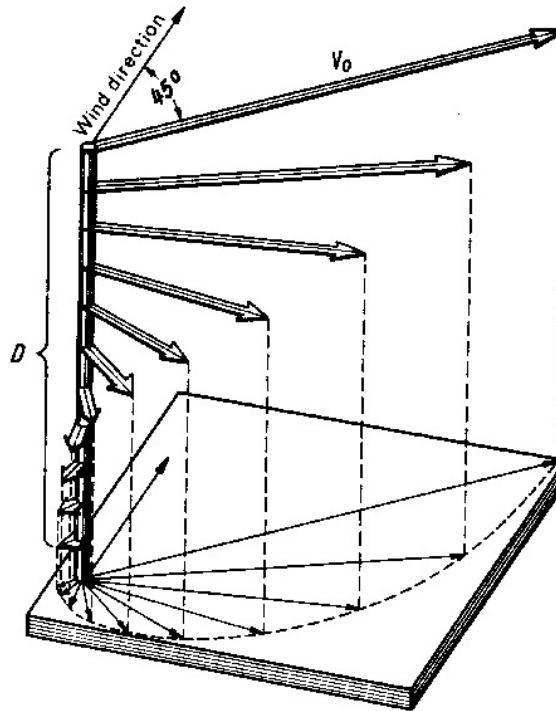


Figure 1.2: Ekman spiral.

1.2 The Sverdrup balance

1.2.1 The barotropic vorticity equation

The most common approach to diagnose the oceanic gyre circulation is to derive an equation for the barotropic, that is the vertically-integrated, vorticity. We will develop a series of theories that are all based on this balance, the simplest being the Sverdrup theory. Indeed, as will soon be shown, a leading-order term in the barotropic vorticity equation is the so-called "beta effect", which corresponds to the meridional advection of planetary vorticity βV . Any meridional motion of water masses induces relative vorticity due to the varying Coriolis acceleration with latitude $\frac{df}{dy} =$

β . This term involves the vertically-integrated meridional transport $V = \int_{-h}^{\eta} v dz$, and noting that by continuity $\frac{\partial U}{\partial x} + \frac{\partial V}{\partial y} = 0$ with $U = \int_{-h}^{\eta} u dz$, we can reconstruct from the beta term a streamfunction of the vertically-integrated horizontal transport:

$$\begin{aligned}\frac{\partial \Psi_{BT}}{\partial x} &= V \\ \frac{\partial \Psi_{BT}}{\partial y} &= -U\end{aligned}$$

with Ψ_{BT} the barotropic (or gyre) streamfunction. Hence the gyre circulation can be comprehensively reconstructed from the zonal integration of the barotropic vorticity equation :

$$\begin{aligned}\beta V &= RHS \\ \implies \frac{\partial \Psi_{BT}}{\partial x} &= RHS/\beta \\ \implies \Psi_{BT}(x, y) &= +\frac{1}{\beta} \int_{x_r}^x RHS(x', y) dx'\end{aligned}$$

with RHS the right hand side of the barotropic vorticity equation and x_r a reference longitude where the streamfunction is assumed null. x_r is usually chosen at the eastern boundary because in the western boundary, the barotropic vorticity balance gets far more complex. In this case $x < x_r$ and we have:

$$\Psi_{BT}(x, y) = -\frac{1}{\beta} \int_x^{x_r} RHS(x', y) dx'$$

Let us first derive the full barotropic vorticity equation from the Boussinesq momentum equations, in order to identify all the terms that can potentially induce a gyre circulation. We recall the momentum equations derived in Chapter 2:

$$\frac{\partial u}{\partial t} + (\mathbf{u} \cdot \nabla)u - fv = -\frac{1}{\rho_0} \frac{\partial P}{\partial x} + \nabla_{\mathbf{h}} \cdot (\kappa_{hu} \nabla_{\mathbf{h}})u + \frac{\partial}{\partial z} (\kappa_{zu} \frac{\partial u}{\partial z}) \quad (1.1)$$

$$\frac{\partial v}{\partial t} + (\mathbf{u} \cdot \nabla)v + fu = -\frac{1}{\rho_0} \frac{\partial P}{\partial y} + \nabla_{\mathbf{h}} \cdot (\kappa_{hv} \nabla_{\mathbf{h}})v + \frac{\partial}{\partial z} (\kappa_{zv} \frac{\partial v}{\partial z}) \quad (1.2)$$

Integrating vertically both equations and cross-derivating $\frac{\partial \int (1.2) dz}{\partial x} - \frac{\partial \int (1.1) dz}{\partial y}$ yields the barotropic vorticity equation:

$$\begin{aligned}\frac{\partial \zeta_{BT}}{\partial t} + Curl \left[\int_{-h}^{\eta} (\mathbf{u} \cdot \nabla) \mathbf{u}_{\mathbf{h}} dz \right] + \beta V &= -\frac{1}{\rho_0} Curl \left[\int_{-h}^{\eta} \nabla_{\mathbf{h}} P dz \right] + Curl \left[\int_{-h}^{\eta} \nabla_{\mathbf{h}} \cdot (\kappa_{hu} \nabla_{\mathbf{h}}) \mathbf{u}_{\mathbf{h}} dz \right] + \frac{Curl(\tau)}{\rho_0} \\ \iff \frac{\partial \zeta_{BT}}{\partial t} + Curl(\mathbf{A}) + \beta V &= \frac{1}{\rho_0} J(P_b, h) + Curl(\mathbf{D}_{\mathbf{h}}) + \frac{1}{\rho_0} Curl(\tau)\end{aligned}$$

with $\zeta_{BT} = \frac{\partial V}{\partial x} - \frac{\partial U}{\partial y}$ the barotropic vorticity, $J(a, b) = \frac{\partial a}{\partial x} \frac{\partial b}{\partial y} - \frac{\partial a}{\partial y} \frac{\partial b}{\partial x}$ the Jacobian operator, P_b the bottom pressure, $\mathbf{A} = \left[\int_{-h}^{\eta} (\mathbf{u} \cdot \nabla) \mathbf{u}_{\mathbf{h}} dz \right]$ and $\mathbf{D}_{\mathbf{h}} = \left[\int_{-h}^{\eta} \nabla_{\mathbf{h}} \cdot (\kappa_{hu} \nabla_{\mathbf{h}}) \mathbf{u}_{\mathbf{h}} dz \right]$ the compact notation of advection and horizontal turbulent diffusion. We have used the continuity equation to simplify the Coriolis term, used Leibniz's integration theorem and neglected sea level variations to simplify the pressure term. Hence once the gyre circulation has reached a steady state, $\frac{\partial \zeta_{BT}}{\partial t} = 0$ and we can diagnose its circulation as:

$$\begin{aligned}V &= \frac{1}{\beta} \left[-Curl(\mathbf{A}) + \frac{1}{\rho_0} J(P_b, h) + Curl(\mathbf{D}_{\mathbf{h}}) + \frac{1}{\rho_0} Curl(\tau) \right] \\ \implies \Psi_{BT}(x, y) &= -\frac{1}{\beta} \int_x^{x_r} \left[-Curl(\mathbf{A}(x', y)) + \frac{1}{\rho_0} J(P_b(x', y), h(x', y)) + Curl(\mathbf{D}_{\mathbf{h}}(x', y)) + \frac{1}{\rho_0} Curl(\tau(x', y)) \right] dx'\end{aligned}$$

Most of the work has been done regarding the gyre circulation with this last equation, because it describes all the physical contributions that can drive or modulate it. It also has the great advantage of being solvable numerically, provided the forcings to its right hand side are known. It means that the gyre circulation can be reconstructed from observed estimates of those forcings, and that in a numerical model the physical drivers of any gyre can be analyzed. Note that $\zeta_{BT} = \Delta_h \Psi_{BT}$, so that a cyclonic gyre will have a positive curvature of the barotropic streamfunction, that is a negative streamfunction, and reversely for an anticyclonic gyre. Physically, the equation states that the gyre circulation is set by the equilibration of the beta effect with:

- The vorticity of momentum advection $-Curl(\mathbf{A})$;
- The interaction of bottom pressure with bathymetry $\frac{1}{\rho_0} J(P_b, h)$ (the so-called bottom pressure torque);
- The vorticity of lateral dissipation $Curl(\mathbf{D}_h)$;
- The wind stress (and/or bottom stress) curl: $\frac{1}{\rho_0} Curl(\boldsymbol{\tau})$.

1.2.2 Sverdrup's hypotheses and equation

The hypotheses of Sverdrup's theory are very similar to those of Ekman, with three notable exceptions:

- No horizontal homogeneity is assumed, precisely because it aims at predicting the horizontal structure of the gyre. However, advection and lateral turbulent diffusion of momentum are assumed negligible (linear and inviscid hypotheses);
- The hypothesis of constant κ_{zu} is withdrawn, because it is unnecessary to predict vertically-integrated transports.
- Because the momentum equations are integrated down to the bottom, two assumptions are necessary to neglect the role of bathymetry: no bottom friction $\boldsymbol{\tau}_b = \mathbf{0}$ and flat bottom $\nabla_h h = \mathbf{0}$.

Hence the momentum equations are identical to the leading-order balance found in Chapter 2, which only includes geostrophic and Ekman dynamics:

$$-f\mathbf{k} \times \mathbf{u}_h = -\frac{1}{\rho_0} \nabla_h P + \frac{\partial}{\partial z} (\kappa_{zu} \frac{\partial \mathbf{u}_h}{\partial z})$$

From the full development of the vorticity equation done above, it is trivial to deduce the Sverdrup balance:

$$\beta V = \frac{1}{\rho_0} Curl(\boldsymbol{\tau})$$

which yields after zonal integration the predicted barotropic streamfunction:

$$\Psi_{BT}(x, y) = -\frac{1}{\rho_0 \beta} \int_x^{x_r} Curl(\boldsymbol{\tau}(x', y)) dx'$$

The great success of Sverdrup theory stems in the fact that it was the first to correctly predict the location of the main subtropical and subpolar gyres. Indeed, over a given basin, the sign of the average wind stress curl at a given latitude gives the correct direction for the meridional flow in the interior ocean. At subtropical Northern latitudes, the negative curl is consistent with average southward flow in the interior (Fig.1.3), that is positive values of Ψ_{BT} . Reversely at subpolar Northern latitudes, the positive curl is consistent with average northward flow in the interior, that is negative values of Ψ_{BT} . It also gives reasonable quantitative predictions for the interior transport of subtropical gyres.

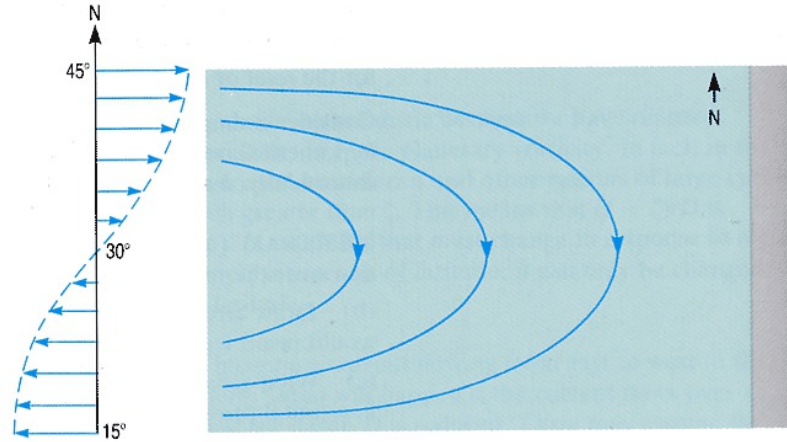


Figure 1.3: Zonal wind stress used in Sverdrup's model (left) and streamlines when integrating from the eastern boundary.

Exercise: estimation of the Sverdrup transport of North Atlantic and Pacific subtropical and subpolar gyres. We assume that the Atlantic basin has a width $W \simeq 6000\text{km}$ with purely zonal winds of $u_{10m}(10^\circ\text{N}) = -5\text{m/s}$, $u_{10m}(40^\circ\text{N}) = +10\text{m/s}$ and $u_{10m}(75^\circ\text{N}) = 0\text{m/s}$ varying linearly between those latitudes. Deduce from the Sverdrup relation the integral meridional transport at 30°N and 60°N . Do the same in the Pacific, assuming the same wind profile and $W \simeq 8000\text{km}$. We assume $C_D \sim 2 \times 10^{-3}$, $\rho_a \sim 1\text{kg/m}^3$, $\rho_0 \sim 1000\text{kg/m}^3$, $\beta(30^\circ\text{N}) \simeq 2 \times 10^{-11}\text{m}^{-1}\text{s}^{-1}$, $\beta(60^\circ\text{N}) \simeq 10^{-11}\text{m}^{-1}\text{s}^{-1}$.

The zonal integration of the Sverdrup relation yields: $\Psi_{BT}(30^\circ\text{N}) = \frac{-1}{\rho_0\beta(30^\circ\text{N})} \int_{x_w}^{x_E} \text{Curl}(\tau) dx = \frac{W}{\rho_0\beta(30^\circ\text{N})} \frac{\partial \tau_x}{\partial y} = \frac{Cd\rho_a W}{\rho_0\beta(30^\circ\text{N})} \frac{u_{10m}^2(30^\circ\text{N}) + u_{10m}^2(60^\circ\text{N})}{L} \sim +20\text{Sv}$ and similarly we get $\Psi_{BT}(60^\circ\text{N}) \sim -40\text{Sv}$. Once again, a gyre of negative vorticity will have positive values of its streamfunction, and vice versa for a cyclonic gyre. Although we get the right sign and order of magnitude for the basin-integrated gyre circulation, we largely underestimate it, which is a typical bias of Sverdrup theory. In the Pacific, the higher basin width by 25% mechanically induces a stronger basin-integrated Sverdrup transport by 25%.

However, due to its extreme simplifications, the Sverdrup theory poses a series of issues. It is known to fail in representing the western side of gyres and subpolar gyres (Fig.1.4), which highly limits its domain of validity. Also, it tends to largely underestimate (typically by a factor ~ 3) the magnitude of both subtropical and subpolar gyre transports (Fig.1.4c). Most importantly, it does not predict any return flow for the gyres, which is however required by continuity. In particular, it does not predict whether the return flow must occur in the eastern or western boundary: the integration of the Sverdrup relation from either the eastern or western boundary gives identical results in the interior. Hence other ingredients must be added to the vorticity balance to permit that return flow.

1.2.3 Interpretation in terms of Ekman and geostrophic flow

The Sverdrup balance strictly results from Ekman and geostrophic dynamics, so that it can be decomposed into two vorticity balances, one within the Ekman layer and the other within the

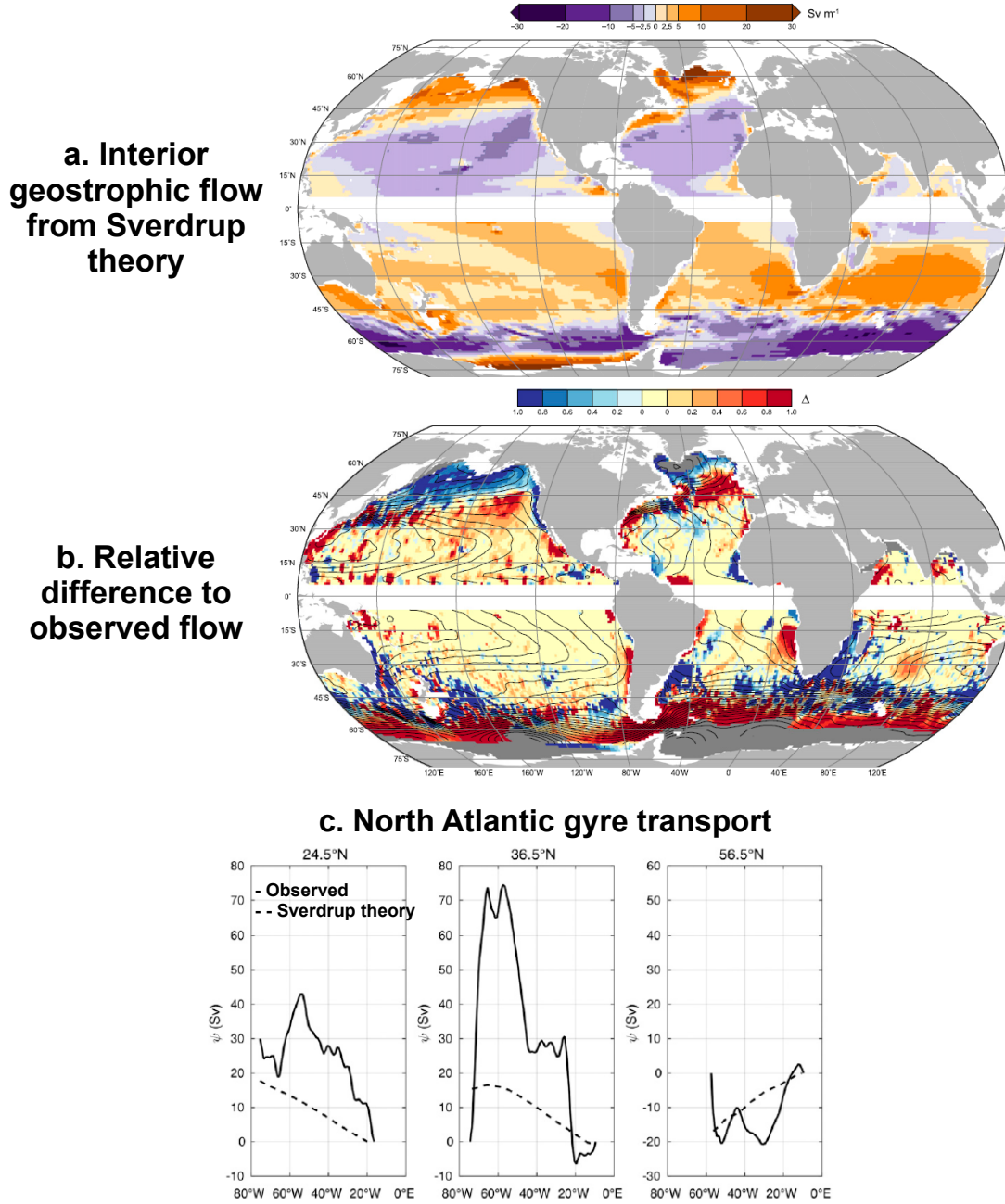


Figure 1.4: a) Interior geostrophic transport predicted from Sverdrup theory and b) relative error (from $-1 = -100\%$ to $+1 = +100\%$) with respect to ARGO measurements (source: Gray and Riser 2014). c) Zonal integration of the gyre transport at specific North Atlantic latitudes, either observed or from Sverdrup theory (source: Colin de Verdière 2016).

geostrophic interior. In the Ekman layer the vertically-integrated vorticity equation writes as:

$$\begin{aligned} \beta V_E + f \int_{-h_E}^{\eta} \nabla_{\mathbf{h}} \cdot \mathbf{u}_{\mathbf{h}} dz &= \frac{1}{\rho_0} \text{Curl}(\boldsymbol{\tau}) \\ \implies \beta V_E - f(w(0) - w(-h_E)) &= \frac{1}{\rho_0} \text{Curl}(\boldsymbol{\tau}) \\ \implies \beta V_E + fw(-h_E) &= \frac{1}{\rho_0} \text{Curl}(\boldsymbol{\tau}) \end{aligned}$$

One additional term appears that was not apparent in the vertically-integrated vorticity equation: the planetary vortex stretching $f w(-h_E)$. It results from planetary vorticity just like the beta effect, and it is related to the conservation of planetary angular momentum: any positive stretching of a water column induces positive vorticity, and vice versa for negative stretching. It cancels out when integrating over the full water column, but it acts as a vorticity coupling between the Ekman layer and the interior ocean. Indeed, in the latter we have the geostrophic vorticity balance:

$$\begin{aligned} \beta V_g + f \int_{-h}^{-h_E} \nabla_{\mathbf{h}} \cdot \mathbf{u}_{\mathbf{h}} dz &= 0 \\ \implies \beta V_g - f(w(-h_E) - w(-h)) &= 0 \\ \implies \beta V_g &= f w(-h_E) \end{aligned}$$

Hence the wind stress imparts vorticity into the Ekman layer, most of which is transmitted to the geostrophic interior ocean by the stretching induced by the Ekman pumping. It can only be equilibrated in the geostrophic interior by the beta effect, which ultimately equilibrates the surface forcing (Fig.1.5). The sum of both balances yields the Sverdrup relation:

$$\beta V_E + \beta V_g = \beta V = \frac{1}{\rho_0} \text{Curl}(\boldsymbol{\tau})$$

which is equivalent to the wind stress decomposition:

$$-\frac{\beta}{\rho_0 f} \tau_x + \frac{f}{\rho_0} \text{Curl}(\boldsymbol{\tau}/f) = \frac{1}{\rho_0} \text{Curl}(\boldsymbol{\tau})$$

Hence, because the first term on the left hand side is relatively smaller, the Sverdrup transport is mostly a response of the geostrophic interior to the wind stress curl. Most importantly, because $f/\beta \sim 10^7 m$, $v_g/w(-h_E) \sim f/(\beta H) \sim 2000$, so that an Ekman pumping as low as $1m/2days$ will induce meridional velocities of $1cm/s$ in the interior ocean. Hence Ekman pumping is important not only for near-surface dynamics, but also for the circulation of the interior ocean.

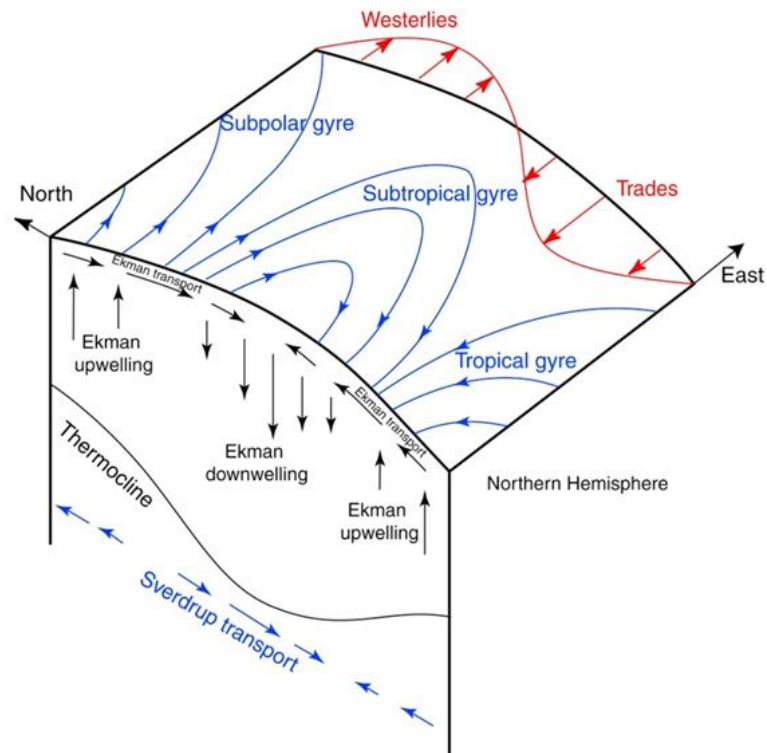


Figure 1.5: Schematic link between wind stress, surface Ekman transport, interior geostrophic transport and gyre circulation (source: Talley et al 2012). The wind stress curl induces a convergence of Ekman transports (Ekman suction) near the surface, which activates an interior southward transport that sets up the Sverdrup balance.

2 The western intensification of gyres

Sverdrup theory explains the weak interior flow of oceanic gyres and the approximate latitude of the subtropical to subpolar separation. However, it does not predict where and how the gyre return flow occurs. Strikingly, this return flow is the only element of the gyre circulation that stands out in an instantaneous map of surface velocities (see Fig.2.2 of Chapter 1). We will see that near the borders, the Sverdrup balance falls apart and other contributions permit an intensified return flow.

2.1 Bottom friction: Stommel model

Although the physics behind Stommel's model is questionable, it was the first one to predict the western return flow of the gyre circulation. He added to Sverdrup balance a bottom friction force modelled as a linear drag on barotropic vorticity: $\tau_b = -r\zeta_{BT} = -r\Delta_h\Psi_{BT}$. Hence the barotropic vorticity equation becomes:

$$\beta V = \frac{1}{\rho_0} \text{Curl}(\tau) - r\Delta_h\Psi_{BT}$$

This allowed him to close the oceanic basin at both the eastern and western borders, and to retrieve an analytical solution for Ψ_{BT} . The resulting circulation illustrates the role played by the beta effect in the western intensification of gyres:

- In the absence of any Earth rotation, an anticyclonic gyre is set into motion by the anticyclonic wind stress, which results in a symmetric circulation (Fig.2.1a). Sea surface height is higher to the northeast and southwest because the water is pushed respectively by westerlies and trade winds, so that zonal pressure gradients balance the zonal wind stress (as is the case in the equatorial ocean).
- In the case of an f plane, the circulation is essentially the same because Coriolis acceleration does not intervene in the barotropic vorticity balance (Fig.2.1b). The main difference is that because of geostrophic equilibration, the sea level essentially follows the circulation streamlines. This is an indication that most of the gyre circulation is at geostrophic balance, as was commented before.
- Now in a beta plane, a zonal asymmetry appears in the circulation and consistently in sea level (Fig.2.1c). Indeed, to the east, the cyclonic beta effect partially compensates the anticyclonic wind stress, so that less bottom friction is needed for the flow to reach a vorticity balance. As friction is proportional to vorticity, this means that the flow must slow down. Reversely, to the west, both the beta effect and the wind stress impart anticyclonic vorticity. Hence the bottom friction must be enhanced to balance both terms. This is done through the intensification of the northward flow. As the basin is closed, by continuity the northward and southward transports must be equal, which implies a narrow western boundary northward flow and a wide interior southward flow.

This model explains most of the gyre structure and asymmetry. Essentially, the explanation in terms of vorticity balance is valid: because of the beta effect, an enhanced cyclonic vorticity source is needed at the western boundary, and a weakened one in the interior ocean. His addition of a bottom friction that opposes the flow explains in particular why the return flow cannot occur at the eastern boundary. However, bottom velocities would need to be unrealistically large for this bottom friction to have a significant role in the vorticity balance. Also, the predicted western boundary current is far too narrow compared to observations. Hence another candidate must be found.

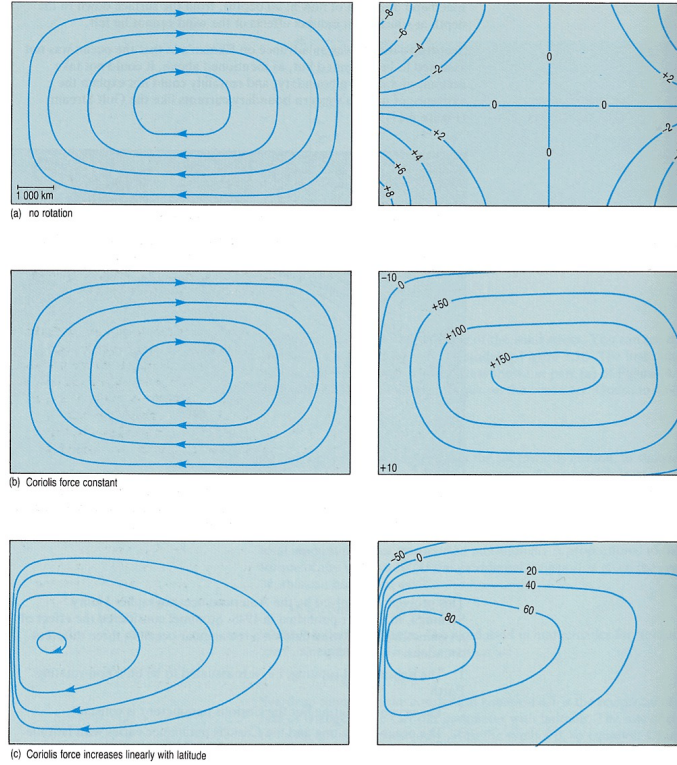


Figure 2.1: Results from Stommel's model : streamlines (left) sea surface height (right) in three idealized cases : no Earth rotation ($f = 0$, top), f plane ($f = f_0$, middle) and beta plane ($f = f_0 + \beta y$, bottom).

2.2 Lateral friction: Munk model

Munk essentially had the same approach as Stommel, except that instead of bottom friction, he assumed that lateral dissipation plays the role of balancing the vorticity equation and permitting an intense western return flow. In this case, the barotropic vorticity equation becomes:

$$\beta V = \text{Curl} \left[\int_{-h}^{\eta} \nabla_{\mathbf{h}} \cdot (\kappa_{hu} \nabla_{\mathbf{h}}) \mathbf{u}_{\mathbf{h}} dz \right] + \frac{1}{\rho_0} \text{Curl}(\boldsymbol{\tau})$$

He assumed the eddy diffusivity coefficient to be constant: $\kappa_{hu} = A$, so that the lateral diffusion term writes as:

$$\begin{aligned} \text{Curl} \left[\int_{-h}^{\eta} \nabla_{\mathbf{h}} \cdot (\kappa_{hu} \nabla_{\mathbf{h}}) \mathbf{u}_{\mathbf{h}} dz \right] &= A \text{Curl}(\Delta_h U_h) \\ &= A \Delta_h \zeta_{BH} \end{aligned}$$

Hence the barotropic vorticity balance becomes:

$$\beta V = A \Delta_h \zeta_{BH} + \frac{1}{\rho_0} \text{Curl}(\boldsymbol{\tau})$$

Horizontal velocities are assumed null at the border (no-slip boundary condition seen in Chapter 2), so that this lateral diffusivity plays exactly the same role as Stommel's bottom friction: it slows down the gyre circulation. A notable difference is that it acts preferentially along the borders, whereas bottom friction is also active in the interior.

Results are very similar to Stommel's model, with only one major improvement: transports cancel at the borders (Fig.2.2). He also applied a more realistic meridional wind profile. However, like Stommel's model, his lateral dissipation requires unrealistic horizontal velocities at the western boundary to balance the vorticity equation. Hence it also predicts a too narrow western boundary current. We will see that less intuitive terms of the vorticity balance intervene in the western intensification of gyres.

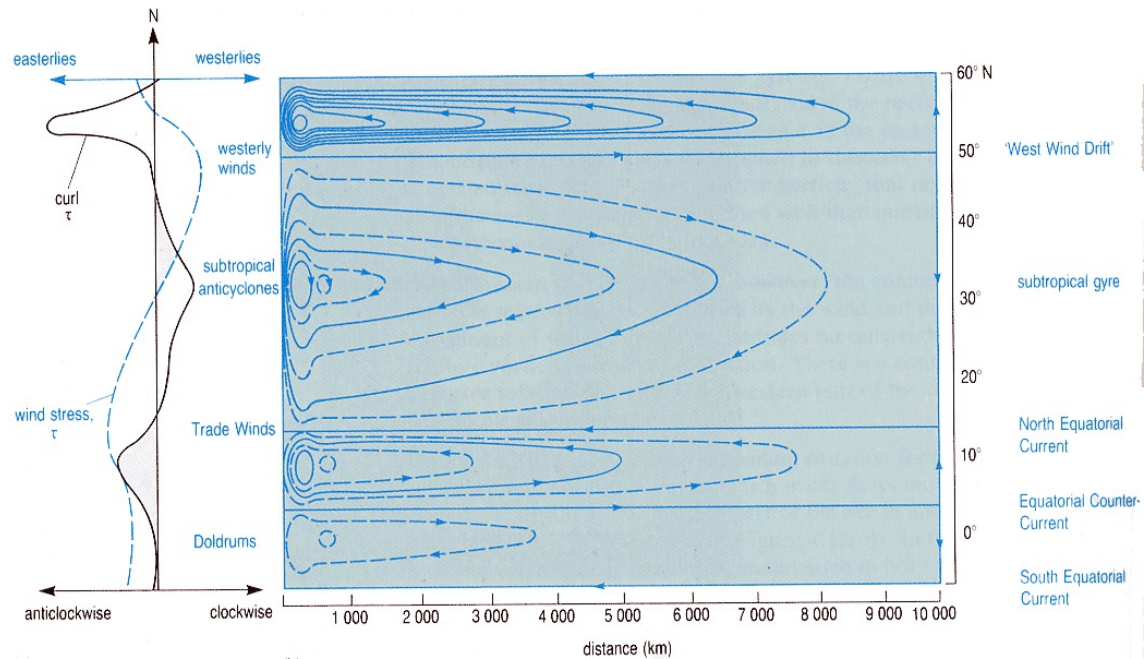


Figure 2.2: Meridional wind and wind stress curl in Munk's model (left) and streamlines of the gyre circulation (right) in an idealized North Atlantic basin.

2.3 Topographic torques

The role of topography appears explicitly in the barotropic vorticity equation as the so-called bottom pressure torque term. As we will see in the barotropic case, its physical effect is to attach the flow to topographic contours, or more precisely to geostrophic f/h contours. Actually, its effect is evident from model simulations of the high-latitude circulation (Fig.2.3), which is relatively barotropic due to the deep-reaching mixed layers. At those latitudes, the beta effect becomes weak so that currents tend to follow closely topography. This topographic control is evident in the Labrador Sea where the main boundary current strictly flows above the $h = 1000m$ isobath (Fig.2.3d). Diagnosis of the full barotropic vorticity balance in an ocean climate model reveals that the bottom pressure torque (Fig.2.3b) is at least as important in determining the gyre circulation (Fig.2.3a) as the wind stress curl (Fig.2.3c), especially for the subpolar gyre.

The simplest derivation of this topographic control on the flow is the formulation of the geostrophic vorticity balance with varying bathymetry $-h(x,y)$ for a barotropic ocean ($\rho = \rho_0$).

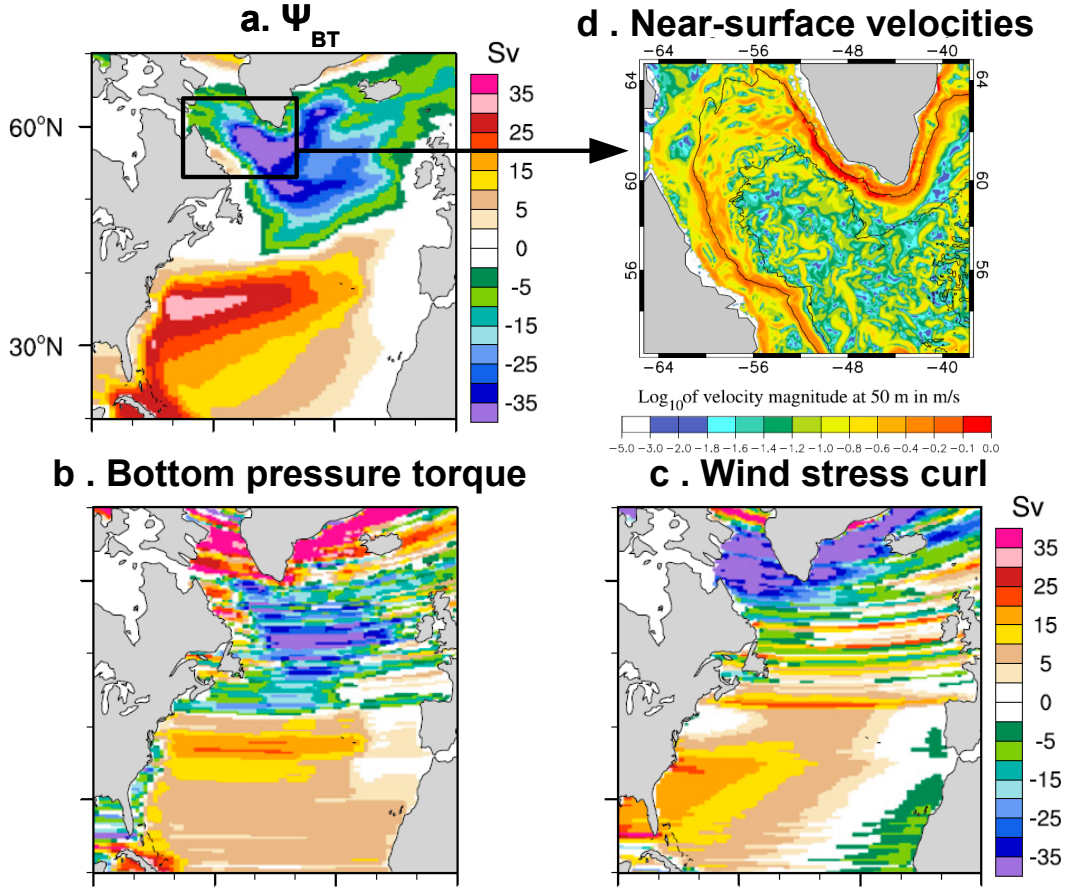


Figure 2.3: a) Barotropic streamfunction in an ocean climate model (1° resolution) and contributions of b) the bottom pressure torque and c) the wind stress curl (source: Yeager 2015). d) Near-surface currents superimposed to the $1000m$ and $3000m$ isobaths (black contours) in the Labrador Sea from an high-resolution ($1/12^\circ$) ocean model (source: Saenko et al 2014). At high latitudes, currents follow topographic contours, which is consistent with the bottom pressure torque dominating the barotropic vorticity balance.

In this case the barotropic vorticity balance becomes:

$$\begin{aligned}
 \beta V &= \frac{1}{\rho_0} J(P_b, h) \\
 &= \frac{1}{\rho_0} \left(\frac{\partial P_b}{\partial x} \frac{\partial h}{\partial y} - \frac{\partial P_b}{\partial y} \frac{\partial h}{\partial x} \right) \\
 &= f(v_g(-h) \frac{\partial h}{\partial y} + u_g(-h) \frac{\partial h}{\partial x}) \\
 &= f \mathbf{u}_g(-h) \cdot \nabla h
 \end{aligned}$$

This development of the bottom pressure torque is general and not specific to a geostrophic and barotropic fluid. It states that whenever the bottom geostrophic velocities push the fluid up or down the topography, it generates vorticity. Indeed, it can be shown mathematically that:

$$J(P_b, h) = 0 \iff P_b = P(h)$$

which means that the bottom pressure torque is null if and only if bottom pressure is constant along isobaths, that is if bottom geostrophic currents follow the isobaths. Hence the bottom pressure

torque is very similar to a bottom vortex stretching that generates positive vorticity when the column is stretched because it is advected down the topography. It can be shown by noting that in the geostrophic case:

$$f\mathbf{u}_g(-h) \cdot \nabla h = f \frac{dh}{dt} = -fw(-h)$$

However physically, the bottom pressure torque is not a vortex stretching: it corresponds to the torque of the force exerted by solid Earth on the ocean bottom. Now remembering that $\beta V = h \frac{df}{dt}$ for a barotropic fluid, we deduce:

$$\begin{aligned} h \frac{df}{dt} - f \frac{dh}{dt} &= 0 \\ \implies \frac{1}{h} \frac{df}{dt} - \frac{f}{h^2} \frac{dh}{dt} &= 0 \\ \iff \frac{d(f/h)}{dt} &= 0 \end{aligned}$$

This expresses the Lagrangian conservation of potential vorticity, which in this simple case is f/h . It has an important consequence for the gyre circulation: bathymetric changes along the flow are sufficient to equilibrate the beta effect induced by any meridional transport. More specifically, a northward flow can be equilibrated if it moves down the bathymetry, and vice versa for a southward flow. This means that a geostrophic circulation can be closed if geostrophic contours f/h are closed, which is the case for much of the North Atlantic subpolar gyre (Fig.2.4). As f contours are purely zonal, a strong meridional deformation of f/h contours means that the topographic slope largely dominates over the beta effect in the barotropic vorticity balance.

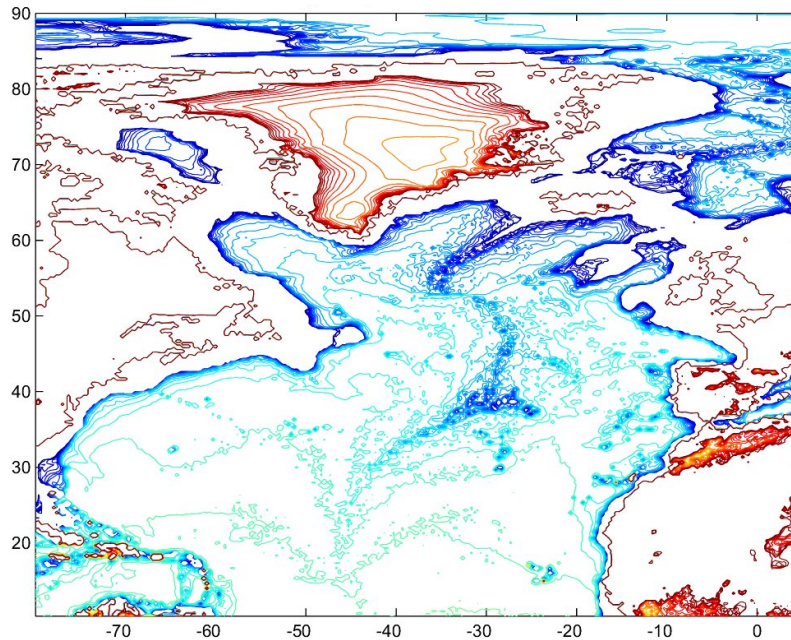


Figure 2.4: North Atlantic geostrophic f/h contours (source: Peter Rhines's lecture). Their large meridional deformation at high latitudes indicates that the flow tends to follow the bathymetry.

If we add the wind stress forcing back to the barotropic vorticity balance we get the so-called topographic Sverdrup balance:

$$\beta V = f\mathbf{u}_g(-h) \cdot \nabla h + \frac{1}{\rho_0} \text{Curl}(\boldsymbol{\tau})$$

This balance states that there is no need of any energy sink such as bottom friction or lateral dissipation to explain the western boundary return flow of gyres. As explained above, it is enough for the western boundary current to flow down the topography as it goes north. In light of recent results, western boundary currents are relatively conservative which means that the bottom pressure torque is a better candidate than bottom friction and lateral dissipation to permit the meridional mass flux in the western boundary. We can also note that in the interior ocean, the bottom pressure torque can also be sufficient to generate a meridional flow, in the absence of any wind stress curl.

Finally, it is worth mentioning that the ocean is generally baroclinic, and in that case the three-dimensional density structure matters, because it determines the bottom pressure torque and hence the circulation. Indeed, the bottom pressure corresponds to the weight of the overlying ocean column. Hence so-called "buoyancy-driven" gyres can exist (Fig.2.5), which are not driven by the wind stress curl but by buoyancy fluxes (heat and water fluxes). This is for instance the case of cyclonic gyres driven by buoyancy loss (cooling or evaporation) in semi-enclosed seas (e.g. the Nordic Seas, Baltic Sea, Mediterranean Sea, Labrador Sea).

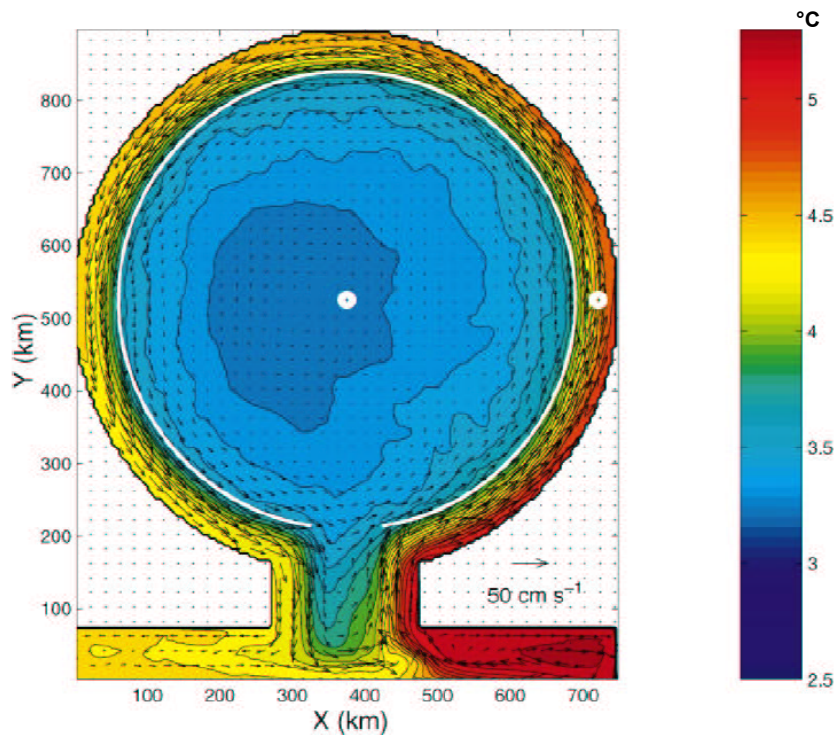


Figure 2.5: Mean surface temperature and velocity of an idealized buoyancy-driven cyclonic gyre driven by no wind stress and a surface heat loss of $Q_{tot} = -200W/m^2$ (source: Spall 2003). Clearly, because of the bottom pressure torque, a surface buoyancy forcing is sufficient to drive a gyre circulation in the absence of any wind forcing.

2.4 Recirculation gyres

So far the only term of the barotropic vorticity balance that has not been analyzed is the so-called non-linear vorticity advection:

$$Curl(\mathbf{A}) = Curl \left[\int_{-h}^{\eta} (\mathbf{u} \cdot \nabla) \mathbf{u}_h dz \right]$$

It includes the lateral advection of relative vorticity and the transfers of vorticity by the relative vortex stretching. It corresponds to the redistribution of vorticity by the ocean in motion. It is referred to as nonlinear advection because, contrary to the planetary vorticity advection $\beta V = \int_{-h}^{\eta} \frac{df}{dt} dz$, it is nonlinear in velocities, meaning that if the flow is quasi-geostrophic, it can be assumed small. However, along the western boundary, velocities become so intense that this term cannot be neglected anymore. Although its net effect is null because it only redistributes spatially the vorticity field, we will show that it explains the presence of intense western recirculation gyres and hence the underestimation of gyre transports by the Sverdrup model.

Let us first characterize the recirculation gyres. Early idealized barotropic simulations with a flat bottom had shown that the reduction of lateral dissipation caused an increase in vorticity advection which in turn could become the leading-order term in the vorticity equation (Fig.2.6). In particular, an intense recirculation gyre was observed offshore of the western boundary current, to the northwestern corner of the gyre (Fig.2.6b). In this recirculation gyre, the barotropic vorticity balance is dominated at the steady state by:

$$\begin{aligned}\beta V &= -\text{Curl} \left[\int_{-h}^{\eta} (\mathbf{u} \cdot \nabla) \mathbf{u}_h dz \right] \\ &= -\mathbf{U} \cdot \nabla \zeta_{BT}\end{aligned}$$

meaning that the advection of planetary vorticity compensates for the advection of relative vorticity (Fig.2.6c). In this Eulerian view, a recirculation gyre can develop if a convergence of anticyclonic vorticity occurs to the east of the boundary current, and reversely to the west. In this case, the equilibration by planetary vorticity advection will cause a southward flow to the east, and a northward flow to the west. With this mechanism, the gyre circulation can be highly intensified without any additional source of energy. This relation can also be interpreted from a Lagrangian point of view. Indeed, the balance between both advective terms is just a consequence of the Lagrangian conservation of potential vorticity, which writes in this flat bottom barotropic case as:

$$\frac{d(hf + \zeta_{BT})}{dt} = 0$$

Hence neglecting the forcing (wind stress) and dissipation (lateral diffusion), the flow must follow geostrophic contours which have constant $hf + \zeta_{BT}$ (Fig.2.6a,b). In most of the domain those contours are blocked by boundaries because they are mostly zonal and dominated by f , and as a consequence water masses cannot circulate freely. This is particularly visible to the southeast which is well dominated by Sverdrup balance and hence where water parcels can only travel south to the extent that wind stress curl permits it (Fig.2.6c). However within the recirculation gyre, because of an intense ζ_{BT} , the potential vorticity is homogenized and water parcels can freely undergo an intense circulation. In this area, the vorticity balance is purely inertial between the beta effect and advection, so that forcing and dissipation become negligible (Fig.2.6c).

Those results are very common to high-resolution ocean models (typically $1/10^\circ$, e.g. Fig.2.7) when compared to their low-resolution counterparts (typically 1°). In the latter the gyre circulation is underestimated and follows closely Sverdrup predictions, whereas in the former gyres intensify by a factor ~ 3 , becoming more realistic and largely departing from Sverdrup balance (Fig.2.7e). In high-resolution models, the respective contributions of transient eddies and the mean flow can even be separated by decomposing the vorticity advection term:

$$\begin{aligned}\beta V &= -\mathbf{U} \cdot \nabla \zeta_{BT} \\ &= -\overline{\mathbf{U}} \cdot \nabla \overline{\zeta_{BT}} - \nabla \cdot \overline{\mathbf{U}' \zeta'_{BT}}\end{aligned}$$

with the classical Reynolds decomposition $X = \overline{X} + X'$ (with X either \mathbf{U} or ζ_{BT}) seen in Chapter 2. Note that only the eddy fluxes $\overline{\mathbf{U}' \zeta'_{BT}}$ that are resolved by the model (typically mesoscale eddies)

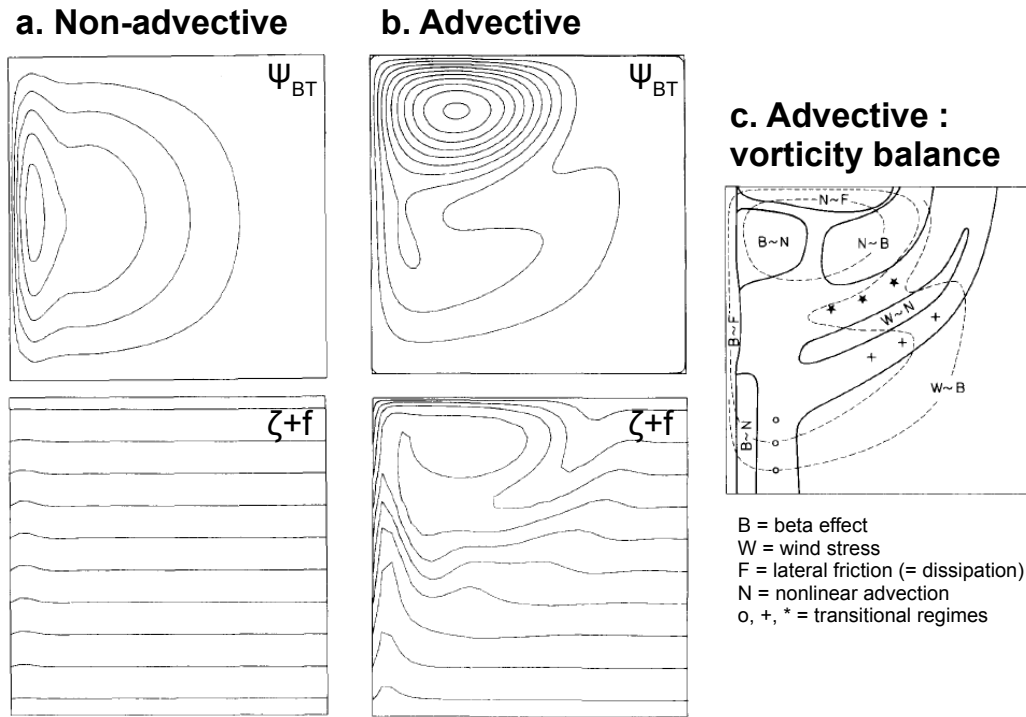


Figure 2.6: Barotropic circulation Ψ_{BT} and potential vorticity contours $\zeta + f$ in an idealized subtropical gyre model a) with weak advection ($\mathbf{A} \propto \mathbf{D}_h/5$) and b) with intense advection ($\mathbf{A} \propto \mathbf{D}_h$) and c) vorticity balance per main dynamical region in the advective case (source: Boning 1986). Note that the authors refer to N as non-linear advection \mathbf{A} and F as lateral friction, which is identical to lateral dissipation \mathbf{D}_h . Vorticity advection creates a northwestern inertial zone which largely increases the gyre circulation.

can be explicitly diagnosed. Results show that both mean and eddy advection are important for these recirculations (Fig.2.7b,c), although once again the bottom pressure torque appears as a key ingredient (Fig.2.7d). Also, both the subtropical and subpolar gyres are concerned by this intensification due to recirculation gyres, mostly along their western boundary currents (Fig.2.7a).

2.5 Eastern shadow zones

The time mean and vertically-integrated view that gyre circulation offers is misleading in several ways. First it does not provide any transient view of how the time-dependent flow sets up and interacts with the gyre circulation. This involves Rossby wave and mesoscale eddy dynamics and will not be developed here. Second it only accounts for transport in the horizontal plane, hence neglecting vertical overturning circulations occurring in the meridional or zonal planes. Those overturning cells largely involve the buoyancy forcing (heat and water fluxes at surface), which do not belong to this chapter. Lastly, and it will be our concern here, the vertical integration gives the misleading feeling that the whole ocean column is ventilated by this gyre circulation. We now try to identify whether some layers in the water column might be unventilated. For that, we must abandon the barotropic vorticity formalism and introduce some depth dependence in the gyre circulation.

First we note that due to Ekman pumping, the trajectory of water masses around the gyres is not horizontal but slanted (Fig.2.8). This slanting is well approximated by the isopycnal slope (slope of density lines) in the interior ocean because there, water parcels are mostly adiabatic

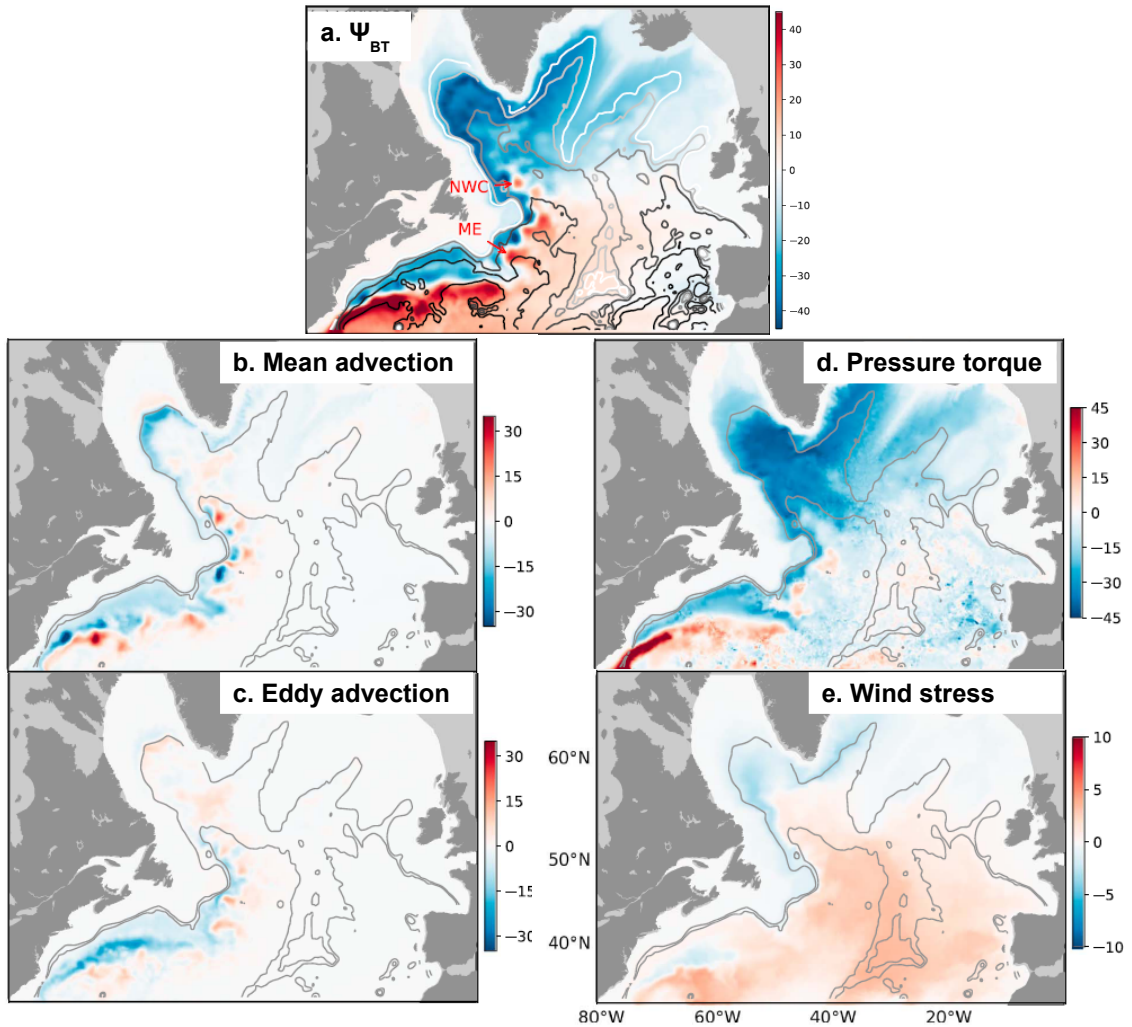


Figure 2.7: a) Barotropic circulation Ψ_{BT} in an eddy-resolving ($1/20^\circ$ resolution) model and contributions of b) mean advection, c) eddy advection, d) bottom pressure torque and e) wind stress curl (source: Wang et al 2017). Most of the subtropical and subpolar gyre circulation is due to an intense western boundary recirculation, which is driven by both vorticity advection and the bottom pressure torque.

and hence they conserve a constant density. This is particularly visible in so-called isopycnal models (vertical levels are density layers, as seen in Chapter 2) because "horizontal" velocities are formulated along isopycnal levels, which are precisely not horizontal (Fig.2.8f). Noting that the meridional gradient of the mixed layer depth is positive (Fig.2.8c), in the interior subtropical gyre, water masses exit the mixed layer (they are subducted, Fig.2.8b) to the north and then they flow southwest while sinking, isolated from surface (Fig.2.8d-f). Such water masses are named mode waters. They can remain for decades below the mixed layer while turning around the subtropical gyre, before resurfacing along the western boundary current (Fig.2.8f). They have a major role in ventilating the interior of subtropical gyres, and they are also a potential source of decadal climate predictability.

The question raised by the so-called "shadow zones" is whether some areas of the interior ocean are not ventilated by those mode waters. The response can be found empirically by noting that subtropical circulation streamlines of mode waters do not reach the southeastern boundary in ocean models (Fig.2.8f) and in observations (Fig.2.9b). Also, the eastern subtropical gyres are

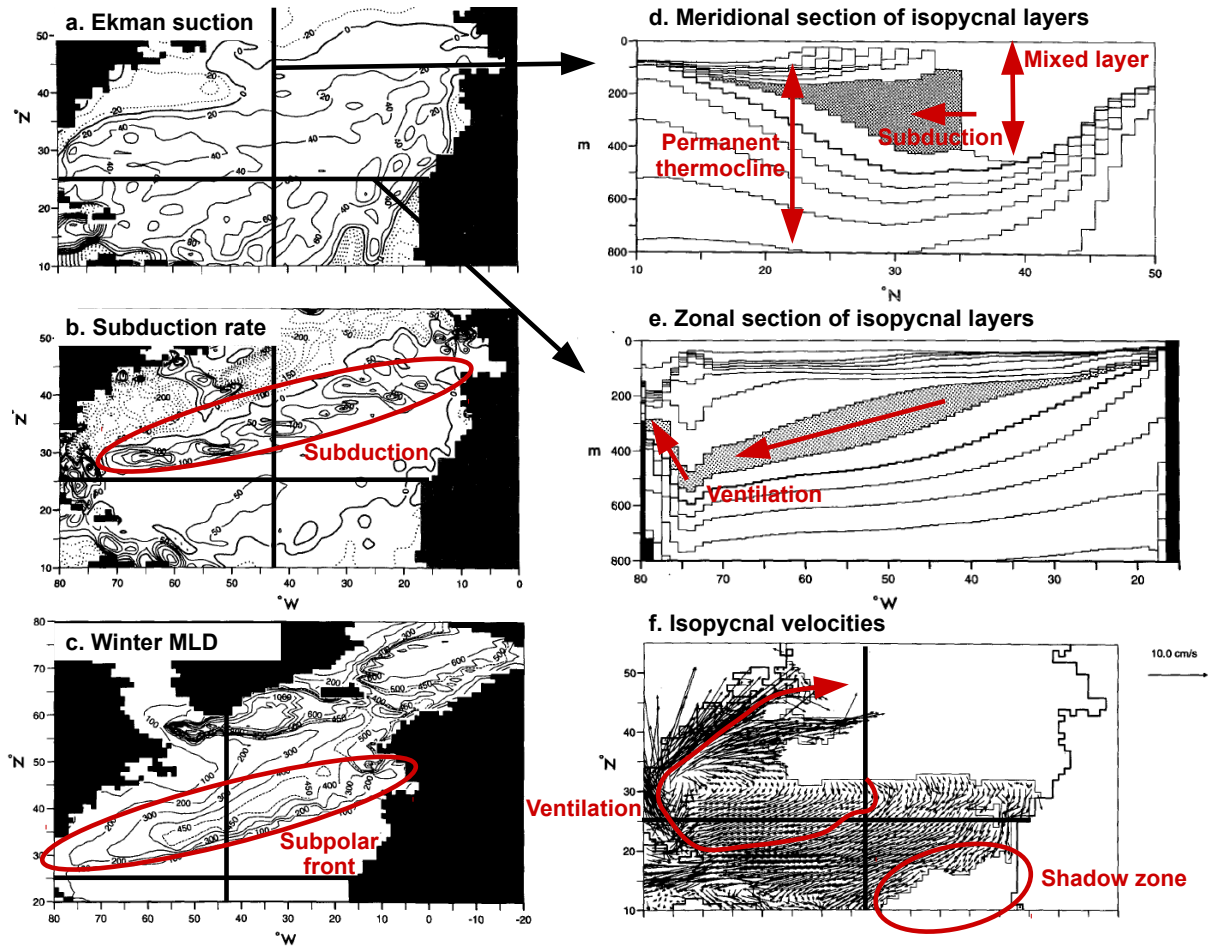


Figure 2.8: Characterization of the gyre ventilation by subduction in an isopycnal ocean model (source: New et al 1995). a) Annual Ekman suction rate ($m/year$), b) annual subduction rate ($m/year$), c) March average mixed layer depth (MLD, m), d) meridional section at $42^\circ W$ and e) zonal section at $35^\circ N$ of isopycnal layer depth (density every $0.15kg/m^3$, $26.70kg/m^3$ layer shaded) and f) isopycnal velocities in the $26.55kg/m^3$ layer. These model results give a clear picture of a slanted gyre circulation which does not ventilate the southeastern corner.

depleted in O_2 (Fig.2.9a), $CFCs$ and nitrate-rich. Although O_2 and nitrate concentrations are also driven by biology, the low CFC concentration is a clear signal of weak ventilation.

The simplest model that gives a physical interpretation to these shadow zones is the so-called 2.5-layer model. It is constituted of two upper layers of constant density in motion, and a lower layer at rest. At some latitude (say $y = y_S$), layer 2 is subducted beneath layer 1 and ventilates the interior ocean while conserving its potential vorticity, which is in this geostrophic case f/h_2 . Hence any southward motion reduces f and must be accompanied by a shoaling of layer 2. At the eastern boundary x_E , this is forbidden by the no normal flow boundary condition: any variation of h_2 along the boundary would induce a zonal flow u_{g2} towards the continent. Hence once water parcels have subducted at the eastern boundary (at the coordinates (x_E, y_S)), they must move southwestward to satisfy both potential vorticity conservation and the no normal flow condition at the eastern boundary. This delimitates a shadow zone which is inaccessible to the gyre circulation. Details of its location can be determined in this simple model by applying Sverdrup balance to both upper layers, and results depend on the structure of the wind stress curl forcing.

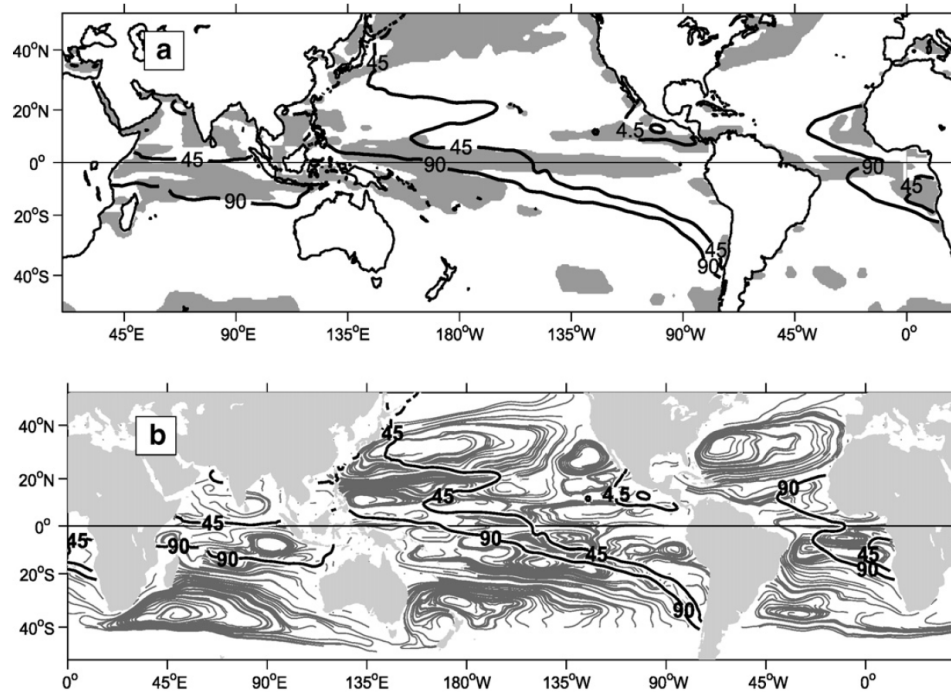


Figure 2.9: Observed O_2 minimum (black contours) in relation to a) main Ekman upwelling regions (shaded grey) and b) mode water trajectories (grey contours) within an isopycnal layer of subtended waters (source: Karstensen et al 2008). The Eastern subtropical O_2 minimum is particularly visible in the North Pacific. The associated Ekman pumping suggests that it is influenced by the overlying biology, but circulation streamlines are consistent with an isolation from the subtropical gyre.

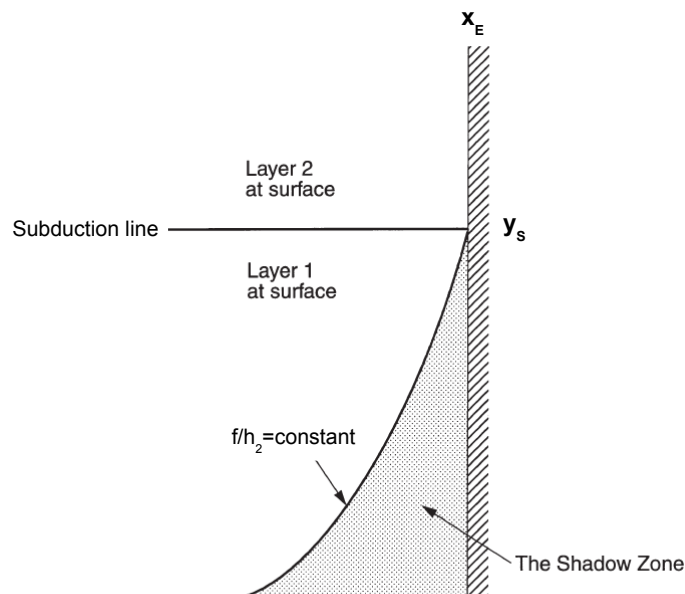


Figure 2.10: Horizontal sketch of the shadow zone in the 2.5 layer geostrophic model (adapted from Vallis 2006). At the eastern boundary x_E , at the latitude y_s where layer 2 is subducted below layer 1, water parcels conserve their geostrophic potential vorticity f/h_2 . This forces them to move southwestward to comply with the no normal flow condition at the eastern boundary.

3 The Southern Ocean circulation

Contrary to other oceanic basins, the Southern Ocean does not display any gyre circulation, with the small exception of the Weddell Sea. Instead, it is dominated by a mostly zonal flow, the Antarctic Circumpolar Current (Fig.3.3a), making the ocean circulation similar to the overlying atmosphere. This is the longest (24,000km) and most intense ($\sim 150Sv$) oceanic current of the world ocean. In addition, the Southern Ocean is the main absorption area of the anthropogenic heat (Fig.3.1) and CO_2 anomalies. We will analyze in the following how its singular circulation relates to the absence of any continental barrier.

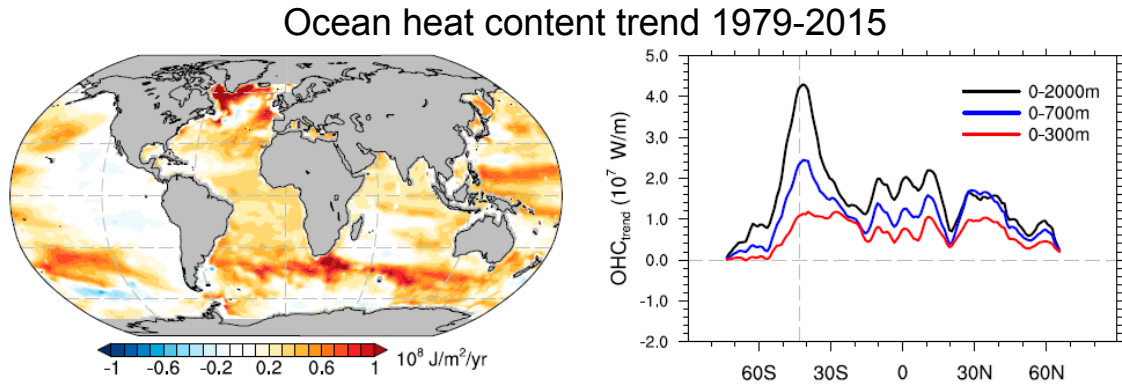


Figure 3.1: 1979–2015 ocean heat content trend map and zonally-integrated as a function of latitude and depth (source: Shi et al 2018). The Southern Ocean stands out as the main heat storage region.

3.1 Meridional overturning: the Deacon Cell

The Southern Ocean circulation is unique in the absence of any zonal boundary. A trivial consequence is the absence of a net meridional flow. Indeed, by continuity, what goes south must balance what comes north, otherwise the sea level would be ever increasing (or decreasing). However, as we will see, this does not prevent intense meridional overturning cells from existing.

3.1.1 Ekman transports

The wind-driven meridional overturning cell is named the "Deacon Cell". Due to the absence of continental obstacles, surface winds are essentially zonal, so that Ekman transports are northward (to the left in the southern hemisphere). In addition, the wind stress curl forms a dipole north and south of the Westerly jet (Fig.3.2b), so that Ekman pumping occurs south, and Ekman suction north of this jet. We have just trivially described three branches of the Deacon Cell (Fig.3.2a), and by continuity we can deduce that there must be a southward geostrophic branch in the interior ocean.

To get insight into the structure of this southward branch, we can write the vorticity balance separately for the surface Ekman layer and the interior geostrophic ocean, as we have done for the gyre circulation. In the Ekman layer it writes, as shown before, as:

$$\beta V_E + fw(-h_E) = \frac{1}{\rho_0} Curl(\tau)$$

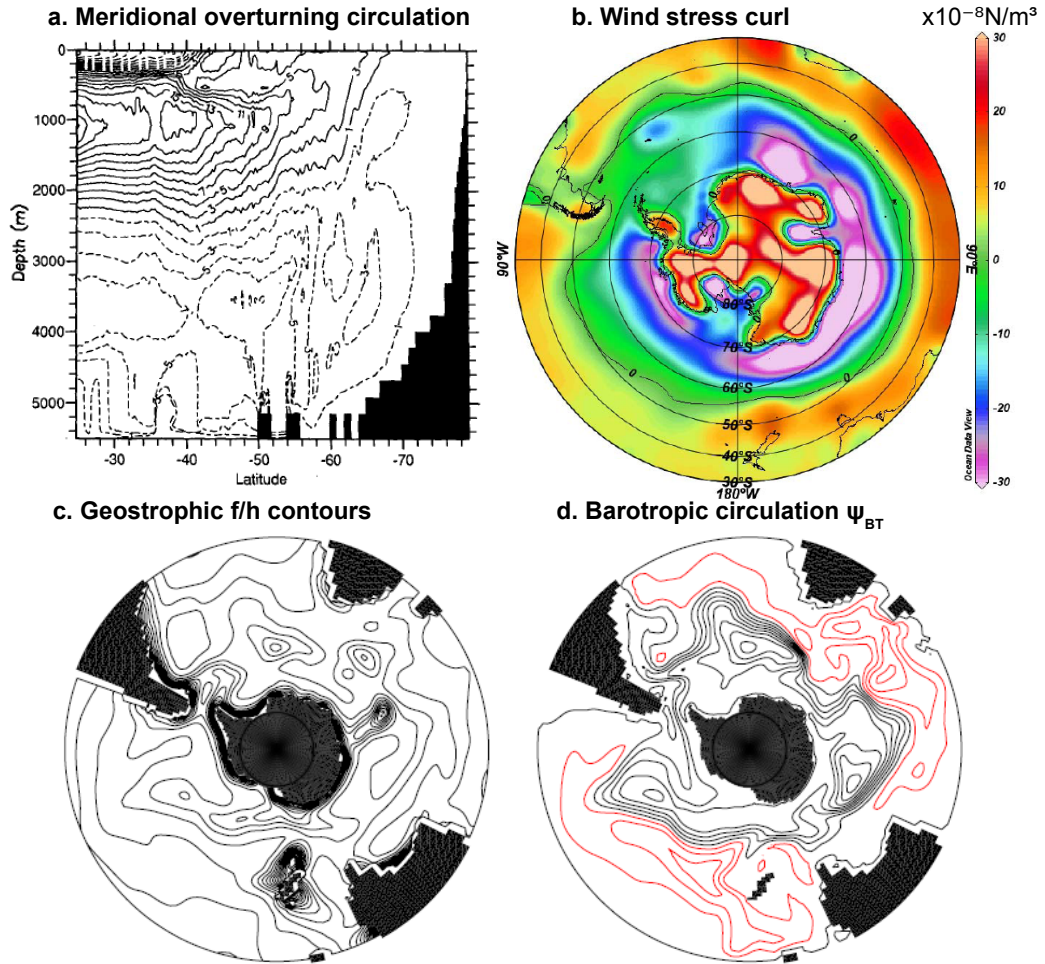


Figure 3.2: Meridional overturning circulation in the Southern Ocean: a) Deacon Cell from an idealized model (source: Doos et al 1994), b) average wind stress curl (source: Leif Thomas’s lecture), c) geostrophic f/h contours and d) barotropic streamfunction Ψ_{BT} from an idealized model (source: Olbers et al 2007). The wind stress curl dipole induces Ekman currents with pumping south and suction north of them, which activates the wind-driven Deacon Cell. The vertically-averaged meridional circulation is null on average but it can locally be intense due to topographic accidents.

This means that part of the wind vorticity input is equilibrated by the beta effect of Ekman currents, and part of it is transmitted to the underlying geostrophic interior by the vortex stretching caused by Ekman pumping.

3.1.2 Meridional geostrophic response

We now turn to the geostrophic vorticity balance that holds in the interior ocean. As seen before, and in the presence of bottom topography, it writes as:

$$\beta V_g = fw(-h_E) + J(P_b, h)$$

The fundamental role of topography can be illustrated by noting that over a zonal integral, we have by continuity:

$$\langle V_E \rangle = - \langle V_g \rangle$$

with $\langle X \rangle = \frac{1}{L_{ACC}} \int_{x_R^-}^{x_R^+} X dx$ the zonal mean of a quantity X over the whole circumpolar zonal ring of length L_{ACC} (with x_R an arbitrary reference longitude). Hence the zonally-integrated vorticity balance of the geostrophic interior writes as:

$$\begin{aligned} \langle \beta V_E + \beta V_g \rangle &= 0 \\ &= \frac{1}{\rho_0} \langle Curl(\boldsymbol{\tau}) \rangle + \langle J(P_b, h) \rangle \end{aligned}$$

Without the bottom pressure torque, the interior ocean could not be in geostrophic balance because there would be no equilibration of the wind stress curl in a zonally-integrated sense. Hence other terms would need to be considered (e.g. vorticity advection, lateral diffusion, bottom friction) and the nature of the flow would be substantially different.

The fact that the geostrophic interior has to lean on the topography to equilibrate the wind stress curl also explains why the Deacon Cell extends very deep in the water column (Fig.3.1a). Indeed, we have seen in the resolution of the Ekman spiral that wind-driven flows are typically very shallow ($h_E \sim 50m$), so that the associated vertical motions do not extend very deep. This coupling mechanism involving the bathymetry in the Deacon Cell is a striking illustration of how some wind-driven flows can ventilate the deep ocean.

3.1.3 Interpreting the barotropic vorticity equation

Why have we not started the analysis of meridional circulation by using the barotropic vorticity equation, as we did for the gyre circulation? Because as was mentioned before, due to the absence of any continental barrier, there can be no net meridional flow across the Southern Ocean. In particular, the Sverdrup balance cannot hold because there is no western boundary to support a northward return flow and hence ensure continuity. If we assume vorticity advection $Curl(\mathbf{A})$ and turbulent horizontal diffusion $Curl(\mathbf{D}_h)$ to be small, the zonal mean barotropic vorticity equation gives:

$$\frac{1}{\rho_0} \langle J(P_b, h) \rangle + \frac{1}{\rho_0} \langle Curl(\boldsymbol{\tau}) \rangle = 0$$

The beta effect is cancelled in the absence of a net meridional flow. Thus although this equation states nothing about the flow, we see once again the importance of the bottom pressure torque and hence of topography. As we have seen before, the strong positive and negative wind stress curls to the north and south of the Westerly jet can be equilibrated by a bottom geostrophic flow going respectively up and down the bathymetry (opposite to the Northern Hemisphere because of negative f).

However, at a given longitude band, some net meridional transport can still occur, which is given by the barotropic vorticity equation. In this case, we have:

$$\beta V = \frac{1}{\rho_0} J(P_b, h) + \frac{1}{\rho_0} Curl(\boldsymbol{\tau})$$

meaning that at a given location along the Antarctic Circumpolar Current, the wind stress curl and above all the bottom pressure torque can generate a net meridional flow. This is the source of the so-called "standing meanders" of the Antarctic Circumpolar Current (Fig.3.1c-d) which, as we will see, play a role in the oceanic meridional heat transfer.

3.2 Mean zonal circulation

How does a zonal wind stress induce a zonal current like the Antarctic Circumpolar Current? This intuitive relation is complicated by the Coriolis acceleration which, at the steady state, induces a

meridional ocean response to a zonal wind. We will also see that the slowdown of the Antarctic Circumpolar Current is due to a non-intuitive mechanism.

3.2.1 Pressure gradient build-up by Ekman transports

Although wind-driven currents (the Ekman currents) are meridional for a zonal wind, they can drive an intense zonal geostrophic flow through the coupling with tracers (temperature and salinity). To illustrate that, let us consider how meridional Ekman transports can intensify a meridional density front. We take the simple case of an initial density gradient of constant value and purely driven by temperature $\frac{\partial \rho}{\partial y}(t=0) = -\alpha_\theta \frac{\partial \theta}{\partial y}(t=0) = -\alpha_\theta \frac{\Delta \theta}{L}$. We assume a purely zonal steady wind stress $\tau = \tau_x(y)\mathbf{i}$ and no heat source $\dot{\Theta} = 0$. In the Ekman layer, the temperature conservation simply writes as:

$$h_E \frac{\partial \theta}{\partial t} = -V_E \frac{\partial \theta}{\partial y}$$

which states that temperature trends are driven by the convergence of the Ekman heat flux. Hence the time evolution of the temperature front is:

$$\begin{aligned} h_E \frac{\partial}{\partial t} \left(\frac{\partial \theta}{\partial y} \right) &= -\frac{\partial}{\partial y} \left(V_E \frac{\partial \theta}{\partial y} \right) \\ &= -\frac{\partial V_E}{\partial y} \frac{\partial \theta}{\partial y} \\ &= -w(-h_E) \frac{\partial \theta}{\partial y} \end{aligned}$$

where we have neglected $\frac{\partial^2 \theta}{\partial y^2}$ and $\frac{\partial h_E}{\partial y}$. We deduce the time evolution of the meridional temperature gradient:

$$\begin{aligned} \frac{\partial \theta}{\partial y}(t) &= \frac{\partial \theta}{\partial y}(t=0) \exp \left[-\frac{w(-h_E)}{h_E} t \right] \\ &= \frac{\Delta \theta}{L} \exp \left[+\frac{\partial \tau_x / f}{\partial y} \frac{\sqrt{f}}{\rho_0 \sqrt{2\kappa_{zu}}} t \right] \end{aligned}$$

Thus where Ekman pumping is negative, that is to the north of the Deacon Cell, Ekman transports will tend to exponentially increase any initial meridional temperature gradient (Fig.3.3). Actually, there is also a dependency to the Ekman depth h_E because for a given Ekman pumping, the thinner the Ekman depth, the stronger the resulting temperature trend within the mixed layer. Because of the meridional gradient of solar radiation, there is always a meridional temperature gradient in the Southern Ocean (Fig.3.3), so that this mechanism is always active. We have just illustrated that Ekman transports can build up a strong meridional density gradient, which will induce in the geostrophic interior the intense zonal Antarctic Circumpolar Current.

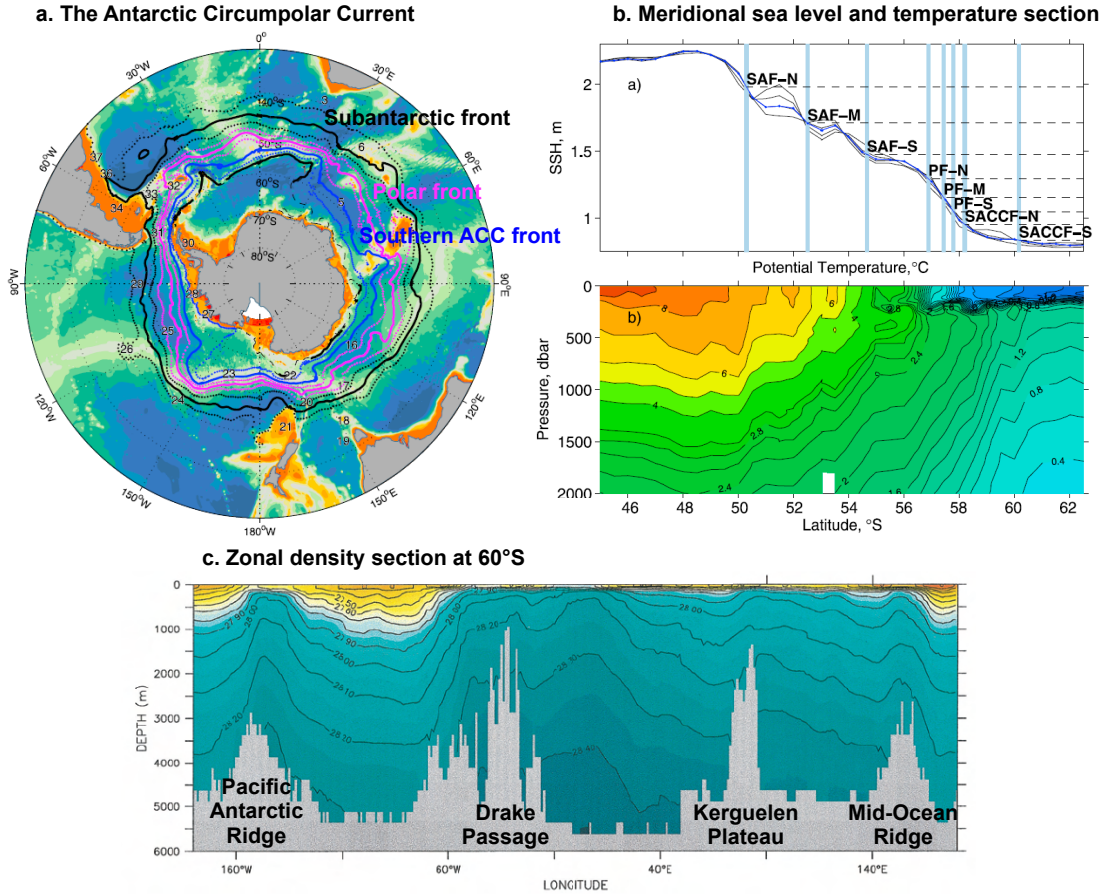


Figure 3.3: Zonal mean circulation in the Southern Ocean: a) the three main fronts of the Antarctic Circumpolar Current (ACC), b) their sea level and temperature signatures (source: Sokolov et al 2009), and c) zonal potential density section at 60°S (source: Olbers et al 2007). The ACC is mostly zonal although it meanders because of topography. It is constituted of three main fronts that have sea level and temperature gradients of same sign, indicating surface-intensified currents. The water column is heavier upstream than downstream of topographic accidents, which slows down the zonal circulation.

3.2.2 Zonal interior geostrophic flow

As there is no zonal Ekman transport, the Antarctic Circumpolar Current is entirely determined by the interior geostrophic flow. The vertically-integrated geostrophic flow writes as:

$$\begin{aligned}
 U_g &= \int_{-h}^{\eta} u_g dz \\
 &= \int_{-h}^{\eta} \left[u_g(-h) + \int_{-h}^z \frac{\partial u_g(z')}{\partial z} dz' \right] dz \\
 &= h u_g(-h) + \int_{-h}^{\eta} \left[\int_{z'}^{\eta} \frac{\partial u_g(z')}{\partial z} dz \right] dz' \\
 &= h u_g(-h) + \int_{-h}^{\eta} z' \frac{\partial u_g(z')}{\partial z} dz'
 \end{aligned}$$

neglecting the sea level variations and using the double integration rule to reverse the order of integrals. This gives with the thermal wind relation:

$$\begin{aligned} U_g &= hu_g(-h) + \frac{g}{\rho_0 f} \int_{-h}^{\eta} z \frac{\partial \rho}{\partial y} dz \\ &\simeq \frac{g}{\rho_0 f} \int_{-h}^{\eta} z \frac{\partial \rho}{\partial y} dz \end{aligned}$$

We have just written the same transport equation as in the Drake Passage exercise of Chapter 2, assuming bottom velocities are small. This diagnostic equation illustrates the coupling between the dynamics and tracers that sets up the Antarctic Circumpolar Current: its intense geostrophic velocities are driven by meridional density (mostly temperature, Fig.3.3b) gradients, themselves enhanced by the Ekman pumping. We must stress that meridional density gradients are also driven by surface buoyancy (heat and water) fluxes.

Meridional density gradients are mostly located near the surface (Fig.3.3b), which makes of the Antarctic Circumpolar Current a surface-intensified current, like most oceanic currents. We can also note that it is constituted of several fronts which delimitate sub-currents at different latitudes (Fig.3.3a-b). Finally, its magnitude relates to its vertical extent which is among the largest for a surface-intensified current (Fig.3.3b). Hence it redistributes globally not only surface waters but also deep waters of the thermohaline circulation.

3.2.3 What slows down the Antarctic Circumpolar Current?

When integrating vertically the zonal momentum equation, the question arises of which physical term slows down the Antarctic Circumpolar Current. Indeed, as we have just seen, it is accelerated by the zonal wind stress, but similarly to the gyre circulation, neither lateral momentum diffusion nor bottom friction are strong enough to equilibrate surface wind stress. This role is played, once again, by the bottom pressure force, through the so-called "bottom form drag". Indeed, the zonally and vertically-integrated zonal pressure force is:

$$\begin{aligned} \left\langle \int_{-h}^{\eta} \frac{\partial P}{\partial x} dz \right\rangle &= \left\langle \frac{\partial}{\partial x} \left(\int_{-h}^{\eta} P dz \right) \right\rangle - \left\langle p(\eta) \frac{\partial \eta}{\partial x} \right\rangle + \left\langle P(-h) \frac{\partial (-h)}{\partial x} \right\rangle \\ &\simeq - \left\langle P(-h) \frac{\partial h}{\partial x} \right\rangle \end{aligned}$$

using Leibniz's integration formula and neglecting sea level variations. Hence for the zonal pressure force to slow down zonal motion, bottom pressure must be on average higher upstream than downstream of seamounts. In this case the pressure force exerted by the seamount on the ocean will be directed westward, hence compensating for the surface wind stress. Because velocities are surface-intensified, bottom pressure gradients are dominated by surface pressure, that is by sea level variations, although they are almost entirely equilibrated by baroclinic pressure gradients so that bottom velocities are small. Hence we have a positive sea level anomaly, although also a negative density anomaly, upstream of the main topographic accidents, and reversely downstream of them (fig.3.3c).

3.3 Role of eddies

3.3.1 Eddy-driven meridional heat transport

Similarly to the atmosphere, the Southern Ocean poleward heat transport is dominated by transient eddies. This is a unique characteristic in the world ocean which transports heat by the mean

circulation (either gyre or overturning) at all other latitudes (Fig.3.4a). Indeed, in the Southern Ocean, the mean meridional circulation is relatively weak and dominated by the Deacon Cell. Within this cell, surface waters are advected equatorward by Ekman currents, whereas colder deep waters are advected southward (Fig.3.4b-c). This induces an equatorward heat transport. On the contrary, eddy heat advection is poleward. The physical mechanism is identical to the atmosphere: transient quasi-geostrophic eddies are formed by baroclinic instability and restratify the ocean, that is, they advect buoyancy (mostly heat, Fig.3.4c) southward. This eddy heat advection occurs half above 200m depth, and half below (Fig.3.4c). Hence eddy heat advection is surface-intensified.

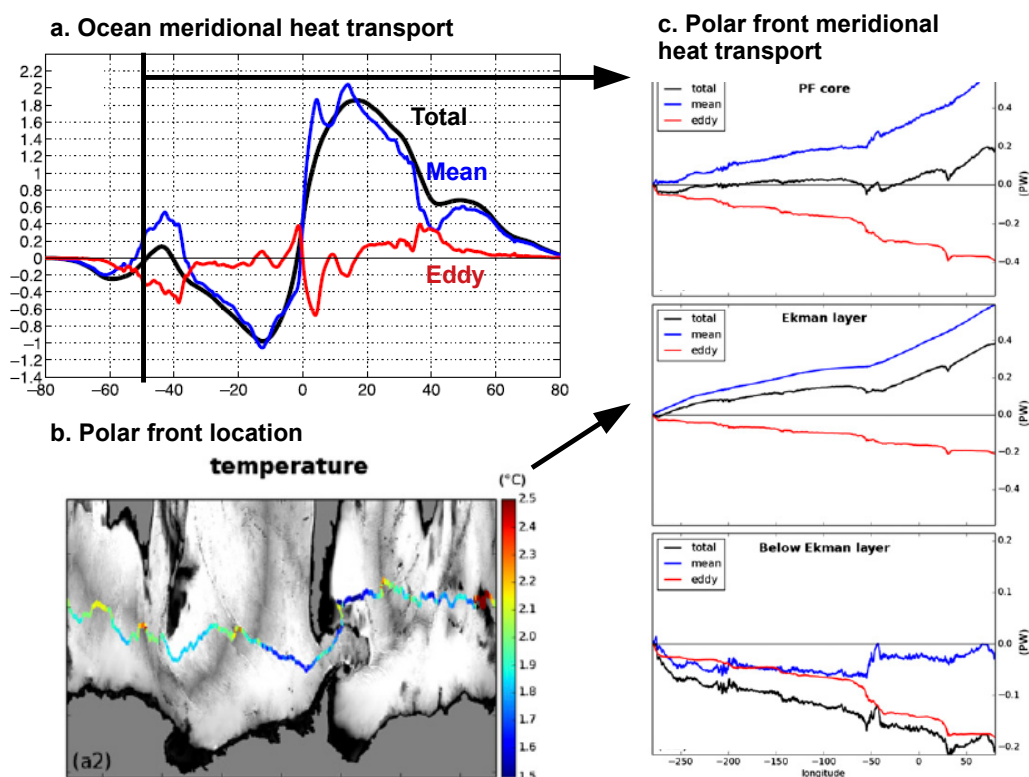


Figure 3.4: a) Meridional heat flux decomposed between the mean and eddy transport in a high-resolution ($1/10^\circ$) ocean model (source: Griffies et al 2015), and b-c) its decomposition as a function of depth and longitude along the Polar Front (source: Duffour et al 2016). The Southern Ocean is singular in that the eddies, not the mean flow, transport heat poleward. The mean flow is due to Ekman transports, whereas the eddy transport is driven by surface-intensified eddies.

3.3.2 Role of standing meanders

Although the meridional heat advection by mean currents occurs on average northward at the latitudes of the Antarctic Circumpolar Current, so-called "standing meanders" can advect heat poleward. To illustrate them, let us decompose mean transports as

$$\overline{\mathbf{U}_h} = \langle \mathbf{U}_h \rangle + \overline{\mathbf{U}_h^*}$$

with $\langle \mathbf{U}_h \rangle$ the zonal mean average transports and $\overline{\mathbf{U}_h^*}$ their zonal anomaly. Similarly we have mean temperatures:

$$\overline{\theta} = \langle \theta \rangle + \overline{\theta^*}$$

Hence neglecting vertical variations of \mathbf{U}_h and θ , we deduce zonally averaged meridional heat transports by standing meanders: $\langle \overline{V^* \theta^*} \rangle$. It happens that meanders advect anomalously cold waters $\overline{\theta^*} < 0$ northward $\overline{V^*} > 0$, and reversely anomalously warm waters southward, so that the zonal mean transport by those meanders is poleward:

$$\langle \overline{V^* \theta^*} \rangle < 0$$

This is simply because waters advected northward come from the south where they have been cooled down by surface heat fluxes, and vice versa for waters coming from the north. However, the Deacon overturning cell still dominates the meridional heat advection by mean currents, so that the net mean heat transport (overturning plus vertical-mean) is equatorward.

3.3.3 Role of transient eddies

Transient mesoscale eddies are ubiquitous in the world ocean. They are particularly intense in baroclinic mid-latitude oceanic regions such as western boundary currents and the Antarctic Circumpolar Current, which indicates their dominant formation through baroclinic instability (Fig.3.5a). Their magnitude is most commonly diagnosed by computing the temporal standard deviation of dynamic sea level. Indeed, this physical parameter is observable from altimetry at a reasonable resolution and its variations are dominated by mesoscale eddies (Fig.3.5b). This is an indication that instantaneous surface geostrophic velocities are dominated by those eddies, as we have seen in Chapter 1.

Transient eddies are mostly created by extraction of available potential energy through baroclinic instability. This means that they advect buoyancy (mostly heat) poleward. Let us first consider the consequences for the meridional flow. First, as we have seen, they play a large role at mid-latitude in ocean meridional heat transports. Second, they induce an meridional overturning transport of buoyancy which is opposed to the Deacon cell, although it is not visible in terms of time mean volume transports. This effect is called the "eddy rectification". It can be quantified with the so-called "transformed Eulerian mean" formalism. The principle is to decompose eddy density fluxes (mostly temperature fluxes) into an isopycnal component that writes as a transport streamfunction and a diapycnal component that write as a diffusivity. To illustrate that let us consider the zonally-averaged mean density equation in the adiabatic ocean interior:

$$\frac{\partial \bar{\rho}}{\partial t} + (\bar{\mathbf{v}} \cdot \nabla) \bar{\rho} + \nabla \cdot \overline{\mathbf{v}' \rho'} = 0$$

where we have decomposed the advection term into the mean and eddy transports, $\mathbf{v} = (v, w)$ and $\nabla = (\frac{\partial}{\partial y}, \frac{\partial}{\partial z})$ denote the zonally-averaged velocities and gradient. Density is conserved, so that its time evolution at a given location is only due to its advection in the meridional plane by mean and eddy velocities. Now let us decompose the eddy transport into a component parallel to isopycnals and another one normal to them:

$$\overline{\mathbf{v}' \rho'} = \chi \nabla_{\perp} \bar{\rho} + K \nabla \bar{\rho}$$

with $\nabla_{\perp} = (\frac{\partial}{\partial z}, -\frac{\partial}{\partial y})$ the rotated gradient operator (90° clockwise to ∇), χ the along-isopycnal eddy transport and K the across-isopycnal eddy transport given by the formulas:

$$\chi = \frac{\overline{\mathbf{v}' \rho'} \cdot \nabla_{\perp} \bar{\rho}}{(\nabla \bar{\rho})^2}$$

$$K = \frac{\overline{\mathbf{v}' \rho'} \cdot \nabla \bar{\rho}}{(\nabla \bar{\rho})^2}$$

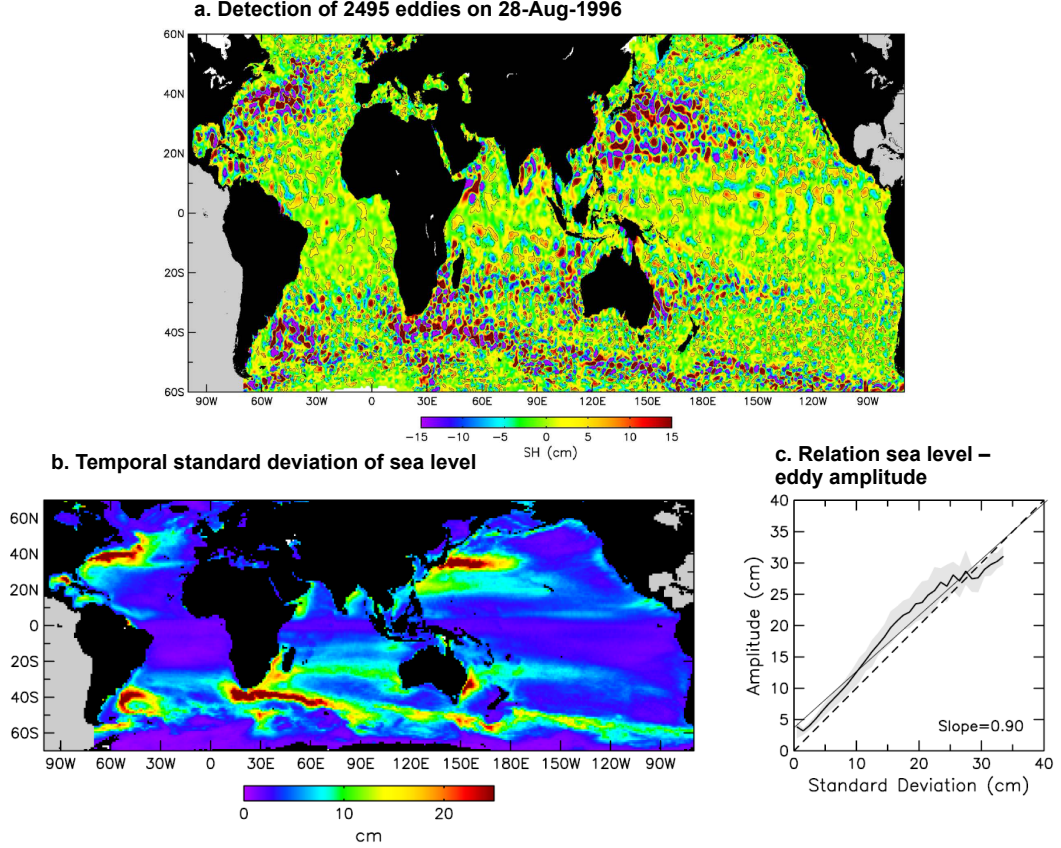


Figure 3.5: a) Snapshot of dynamic sea level on 28-Aug-1996 (shades) and eddy tracking (contours). b) Temporal standard deviation of sea level (high-pass filtered) and c) its spatial scatterplot with the average eddy sea level amplitude (source: Chelton et al 2011). Mesoscale eddies are ubiquitous, especially around the Antarctic Circumpolar Current, and they dominate surface geostrophic velocities.

We have just projected the eddy transport term onto a new coordinate system following density surfaces. Now the interest of this operation is that the eddy transport divergence term of the density equation now writes as:

$$\nabla \cdot \overline{\mathbf{v}'\rho'} = \nabla \cdot (\chi \nabla \bar{\rho}) + \nabla \cdot (K \nabla \bar{\rho})$$

The second term has the form of the usual eddy diffusivity introduced for the closure of turbulence, as we have seen in Chapter 2. However, there is an additional term which does not take the form of a diffusivity. Let us develop it:

$$\begin{aligned} \nabla \cdot (\chi \nabla \bar{\rho}) &= \frac{\partial}{\partial y} \left(\chi \frac{\partial \bar{\rho}}{\partial z} \right) + \frac{\partial}{\partial z} \left(\chi \left(-\frac{\partial \bar{\rho}}{\partial y} \right) \right) \\ &= \frac{\partial \chi}{\partial y} \frac{\partial \bar{\rho}}{\partial z} - \frac{\partial \chi}{\partial z} \frac{\partial \bar{\rho}}{\partial y} \\ &= -\nabla \chi \cdot \nabla \bar{\rho} \end{aligned}$$

This shows that χ is the streamfunction of the eddy-induced transport. Indeed, if we introduce $v^* = -\frac{\partial \chi}{\partial z}$ and $w^* = +\frac{\partial \chi}{\partial y}$, we find the following density equation:

$$\frac{\partial \bar{\rho}}{\partial t} + ((\bar{\mathbf{v}} + \mathbf{v}^*) \cdot \nabla) \bar{\rho} + \nabla \cdot (K \nabla \bar{\rho}) = 0$$

So far we have made no approximation. Our decomposition has just permitted to illustrate that eddy transports take the form of eddy-induced velocities plus eddy diffusivities. Now we must close turbulent terms χ and K to resolve this equation. We first make the so-called "eddy adiabatic" assumption $K = 0$, which states that eddies transport tracers along isopycnals. This allows to introduce only one closure equation (e.g. for $\overline{v'\rho'}$) and deduce the second ($\overline{w'\rho'}$) so that the eddy flux is isopycnal:

$$\begin{aligned}\overline{v'\rho'} &= -\kappa^* \frac{\partial \bar{\rho}}{\partial y} \\ \implies \overline{w'\rho'} &= -\left(\frac{\partial \bar{\rho}}{\partial y} / \frac{\partial \bar{\rho}}{\partial z}\right) \overline{v'\rho'} \\ &= -\kappa^* s \frac{\partial \bar{\rho}}{\partial y} \\ &= +\kappa^* s^2 \frac{\partial \bar{\rho}}{\partial z}\end{aligned}$$

with κ^* the isopycnal eddy diffusivity and $s = -(\frac{\partial \bar{\rho}}{\partial y} / \frac{\partial \bar{\rho}}{\partial z})$ the isopycnal slope. Finally, and thanks to the "eddy adiabatic" hypothesis, we obtain a very simplified expression for χ :

$$\begin{aligned}\chi &= \frac{\overline{v'\rho' \cdot \nabla \bar{\rho}}}{(\overline{\nabla \bar{\rho}})^2} \\ &= \frac{\overline{v'\rho'}}{\frac{\partial \bar{\rho}}{\partial z}} \times \frac{1+s^2}{1+s^2} \\ &= -\kappa^* \left(\frac{\partial \bar{\rho}}{\partial y} / \frac{\partial \bar{\rho}}{\partial z}\right) \\ &= +\kappa^* s\end{aligned}$$

After a lot of pain, we have just formulated the streamfunction that defines the "eddy-induced velocities" introduced in Chapter 2. It is used as a parametrization of eddies in all low resolution ($\sim 1^\circ$) ocean models because it largely improves the mean flow and water mass distribution. Now we know that it only depends on an isopycnal diffusivity κ^* which can be taken either constant or variable, and on the spatial variations of isopycnal slopes. In a high resolution ocean model, it is resolved so that values of κ^* can be determined. Going back to the Southern Ocean, this eddy-induced overturning (Fig3.6c) is opposite to the mean overturning (Fig3.6b), so that the overturning felt by tracers (e.g. temperature), called the residual circulation, is weakened (Fig3.6a). The eddy-induced overturning advects light (warm) waters poleward and dense (cold) waters equatorward, which also explains the intense poleward heat transport by eddies.

Finally, transient eddies also modify the zonal mean flow. As we have seen before, the thermal wind relation states that the magnitude of zonal transports is closely related to meridional gradients of buoyancy. Hence a sink of available potential energy reduces buoyancy gradients and the mean currents. The resulting circulation in the Antarctic Circumpolar Current is weaker than it would be in their absence. This effect is qualified as the "eddy saturation" of the mean zonal flow.

3.4 An energetic interpretation: the oceanic Lorenz Energy Cycle

The Southern Ocean circulation highlights the importance of both the mean and eddy dynamics. For this reason it is very enlightening to analyze the oceanic Lorenz Energy cycle, which describes exchanges between the main reservoirs of mechanical energy (Fig.3.7a). Without developing the

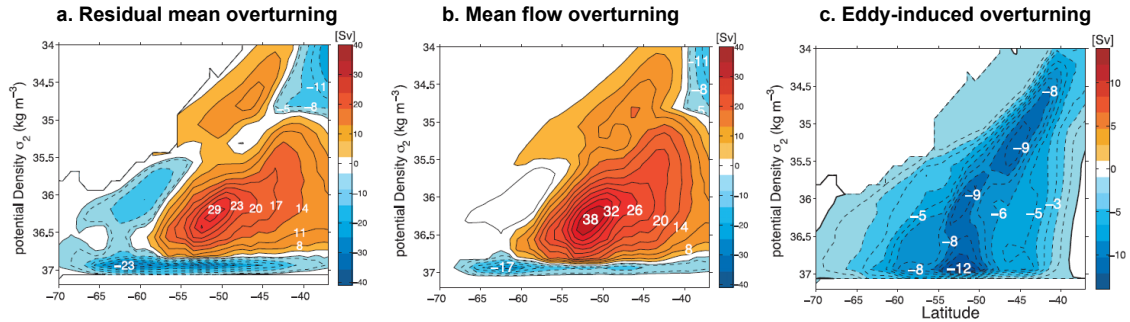


Figure 3.6: Residual mean, mean and eddy-induced meridional overturning diagnosed in the Southern Ocean (source: Farneti et al 2010). The vertical coordinate is density and can be considered similar to depth. Because of transient eddies, the wind-driven overturning is weakened, which transports heat southward and weakens the Antarctic Circumpolar Current.

equations for each reservoir, we define the available potential energy (P) as the gravitational potential energy with respect to a horizontally homogeneous reference state, that is the energy available for baroclinic conversion into kinetic energy. We separate both the P and kinetic energy (K) reservoirs into a mean (P_m and K_m) and eddy (P_e and K_e) component, respectively for the time mean and time-varying contributions.

First we have seen that the mean circulation in the Southern Ocean is set up by the wind forcing. It is evident from the Lorenz energy cycle that wind work ($G(K_m)$) is the main source of K_m . Second we have identified that Ekman pumping builds meridional density gradients, that is P_m : it corresponds to the $C(K_m, P_m)$ flux. P_m can also be directly created by buoyancy (mostly heat) fluxes at surface ($G(P_m)$) which contribute to meridional density gradients. Once this large P_m has been built, it can be converted by baroclinic instability ($C(P_m, P_e)$ and $C(P_e, K_e)$) into K_e which constitutes by far the main kinetic energy reservoir of the ocean. Those eddies have extracted P_m from the system, which corresponds to the meridional heat transport and the rectification of the flow. They can finally transfer kinetic energy to lower scales where it will ultimately have to be dissipated ($D(K_e)$) so that at steady state, sources and sinks of mechanical energy are equal. We note that transfers between K_m and K_e are limited, meaning that neither component drives the other: there is neither intense barotropic instability ($C(K_m, K_e)$) nor an intense inverse cascade ($C(K_e, K_m)$).

Comparison with the atmospheric Lorenz Energy cycle (Fig.3.7b) illustrates striking differences which are due to the different nature of their forcings. In the atmosphere, the forcing is diabatic, so that it increases P_m . From that, atmospheric dynamics must extract this energy through baroclinic conversion to be set into motion. Ultimately, it is the transient eddies that drive the mean circulation through the so-called inverse cascade. In this sense, eddies have a greater role in atmospheric than oceanic circulation, and the atmosphere has a much less forced and more internal dynamical nature than the ocean.

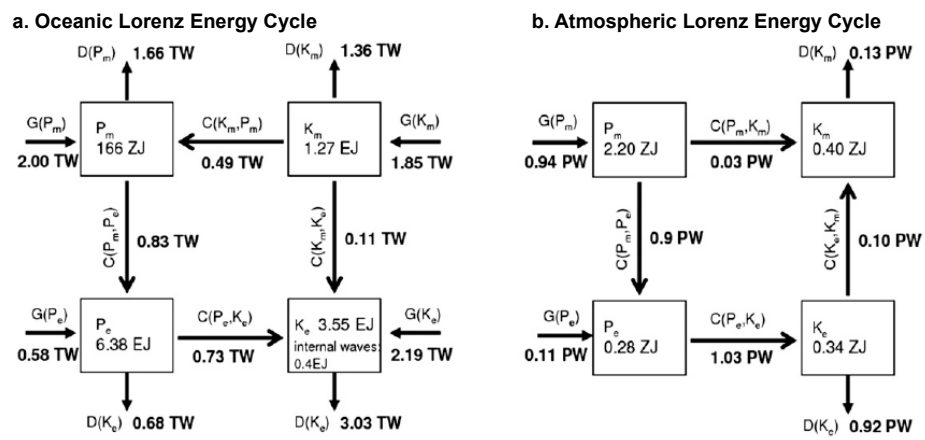


Figure 3.7: a) Oceanic and b) atmospheric Lorenz Energy Cycles deduced from high-resolution simulations (source: von Storch et al 2012). Conversion terms are noted C, generation G and dissipation D. Both fluids are strikingly different owing to the different nature of their forcings.

4 The Tropical circulation

Along the Equator, the ocean dynamics are fundamentally different because the Coriolis acceleration cancels out. This generates very fast waves that make of the ocean and atmosphere a coupled system, contrary to extratropical latitudes. In addition, due to the weakness of the Coriolis force, currents are very strong and unbalanced, with a wind-driven flow extending to higher depth. However, not far from the Equator, geostrophic and Ekman balances are restored, and even in the Equatorial band winds play a determinant role in the circulation. Therefore the circulation remains largely wind-driven and under the effect of rotation. In the following, we will focus our attention, as in the rest of this chapter, on the time mean equatorial circulation, hence excluding modes of variability such as El Niño - Southern Oscillation (ENSO). As a consequence, the time mean circulation described here excludes the anomalous El Niño phase of ENSO and the summer monsoon regimes.

4.1 Meridional circulation

Near the Equator, the meridional circulation is complexified by the strong modulations of Ekman transports. From the maximum trade wind jet (around $\pm 10 - 15^\circ$ of latitude), trade winds weaken to reach the so-called "doldrums" at the Inter-Tropical Convergence Zone (see Fig.2.2). However, the Coriolis parameter also varies rapidly to cancel at the Equator. As we will see, these variations generate the Tropical Gyres, the Tropical Cells and the Subtropical Cells.

4.1.1 Tropical gyres

In the $\sim 5 - 15^\circ$ latitude band, as predicted by Munk (see Fig.2.2), tropical gyres are generated by the positive Ekman pumping due to the poleward intensification of trade winds (Fig.4.1a). Symmetrically to subtropical gyres, the Ekman pumping induces a poleward interior Sverdrup transport (Fig.4.1b) which is returned by an equatorward western boundary current (Fig.4.1c). The subtropical-tropical gyre separation defines the North Equatorial Current, whereas the southern edge of the tropical gyre defines the North Equatorial Countercurrent.

However, Sverdrup theory predicts much weaker transports than what is observed (Fig.4.1b-c). In particular, the North Equatorial Countercurrent is part of the Equatorial current system and largely deviates from Sverdrup balance. Therefore it is mostly unrelated to gyre dynamics simply because Sverdrup theory does not hold anymore near the Equator. In addition, those tropical gyres are a much less steady feature of ocean circulation than their subtropical and subpolar counterparts. The Ekman pumping associated with trade winds almost cancels in the winter of each hemisphere, so that the corresponding tropical gyres also weaken, or even disappear as is the case in the tropical North Atlantic. Finally, trade winds are interrupted by the seasonal to interannual variability associated with ENSO and the monsoon systems, and hence so are the tropical gyres. This last point is true of the tropical circulation as a whole.

4.1.2 Tropical cells

Moving closer to the Equator, in the Deep Tropics ($\pm 5^\circ$ latitude band), the Ekman pumping is not dominated by the wind stress curl (the trade wind weakening) anymore but by the beta effect. In the Equatorial beta plane, the Coriolis parameter is: $f = \beta y \simeq \frac{2\Omega}{R_a} y$ with R_a the Earth's radius.

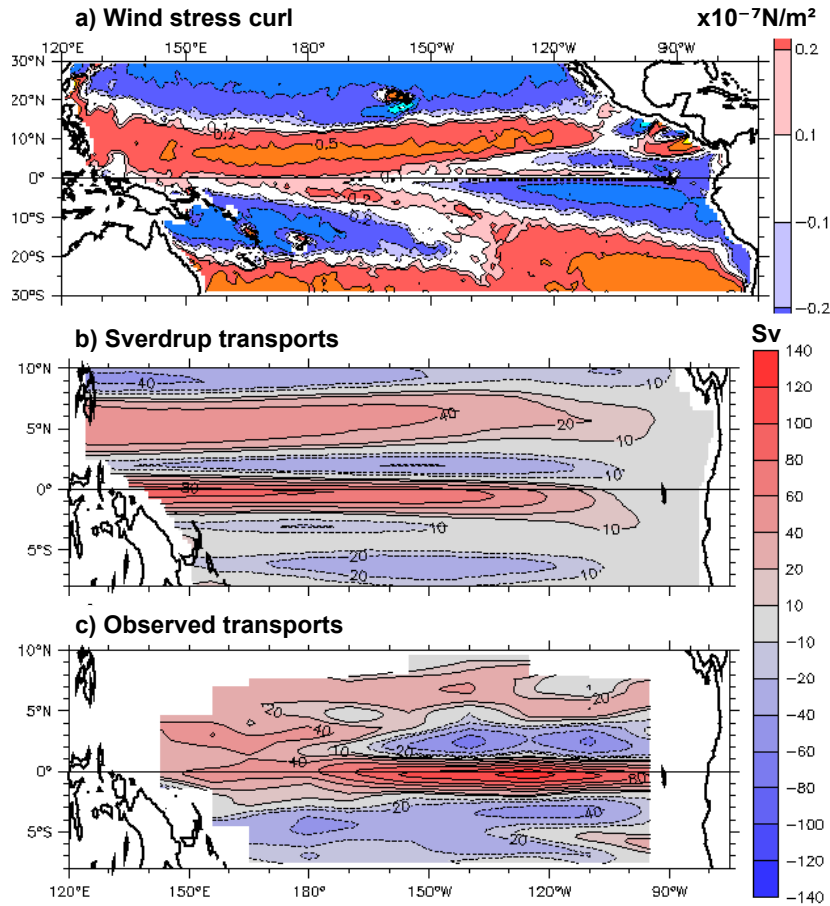


Figure 4.1: a) Observed wind stress curl, b) vertically-integrated transports predicted from Sverdrup theory and c) observed vertically-integrated transports in the Tropical Pacific (source: Kessler et al 2003). Despite a wind stress curl driving a Tropical Gyre on each side of the Equator, the predicted Sverdrup transport is by far underestimated, especially in the Deep Tropics. This is because the geostrophic balance falls apart near the Equator.

Hence the Ekman pumping becomes:

$$\begin{aligned}
 w(-h_E) &= \frac{1}{\rho_0} \text{Curl} \left(\frac{\tau}{\beta y} \right) \\
 &= \frac{1}{\rho_0} \left[\frac{\partial \tau_y / (\beta y)}{\partial x} - \frac{\partial \tau_x / (\beta y)}{\partial y} \right] \\
 &= -\frac{1}{\rho_0} \left[\frac{1}{\beta y} \text{Curl}(\tau) - \frac{\tau_x}{\beta y^2} \right] \\
 &= \frac{1}{\rho_0 \beta y} \left[\frac{\tau_x}{y} - \text{Curl}(\tau) \right]
 \end{aligned}$$

Near the Equator, the first term, that is the beta effect, becomes dominant in the Ekman pumping. Indeed, it becomes more and more difficult for Coriolis acceleration to balance pressure gradients and the surface wind stress. As a consequence, the dynamics deviates significantly from geostrophic and Ekman balances, and stronger currents are required to balance both physical forcings. Hence, the average Ekman pumping becomes negative around 5° of latitude. However, at

the Equator, the Coriolis acceleration cancels out and so do the Ekman transports, so that as we have seen in a previous exercise there is an intense upwelling along the Equator. We have just described, similarly as the Deacon Cell, three branches of a wind-driven meridional cell, one on each side of the Equator. They are the oceanic Tropical Cells (Fig.4.2a). By continuity, just like the Deacon Cell, there should be an interior equatorward return flow. This return flow is also geostrophic because as for Ekman currents, geostrophic balance is restored a few degrees away from the Equator. However, contrary to the Deacon Cell, there are zonal boundaries at the Equator so that this return flow is supported by each basin's zonal pressure gradient. The zonal pressure gradient is itself built up by zonal Equatorial currents driven by trade winds that push warm waters in the so-called western "Warm Pools" (see Fig.4.3 and Fig.4.6).

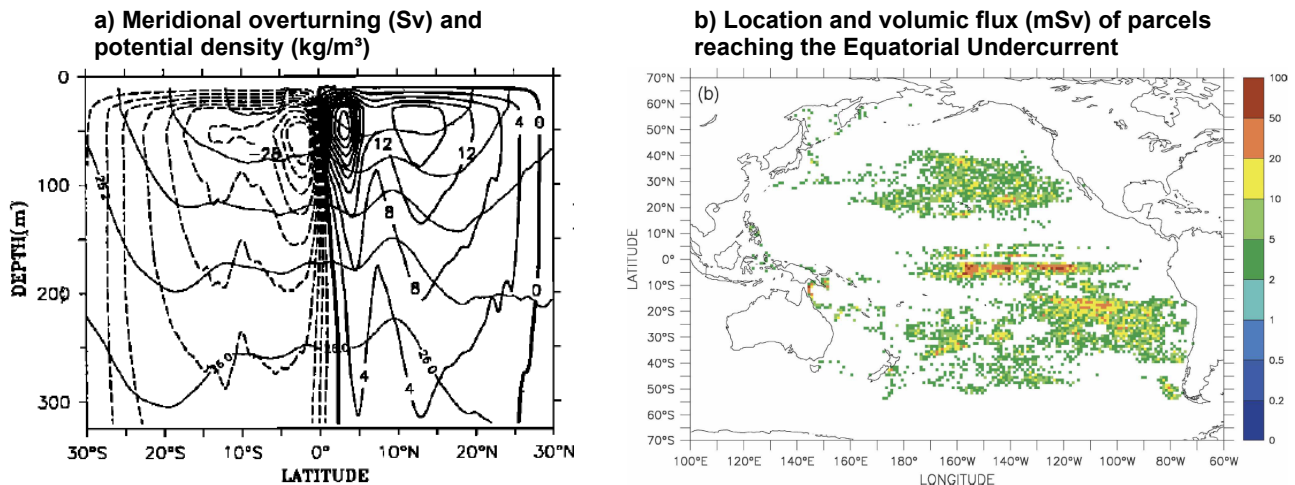


Figure 4.2: a) Meridional overturning streamfunction and potential density section from a numerical model of the Tropical Indo-Pacific (source : Hazeleger et al 2001) and b) location and volumic flux of simulated Lagrangian parcels reaching the Pacific Equatorial Undercurrent (source: Goodman et al 2005). The intense Tropical Cells lie within 5° of the Equator and the more diffuse Subtropical Cells span the whole subtropical band. They both feed the Equatorial Undercurrent, although the latter dominates this equatorward transport.

4.1.3 Tropical Instability Waves

The Deep Tropics are the only region where the ocean dominates over the atmosphere in the meridional heat transport (see Fig.4.7 of Chapter 1). This is due primarily to the Tropical Cells that advect light (warm) surface waters poleward and denser (colder) subsurface waters equatorward (Fig.4.2a). However, there is a striking similarity with the Southern Ocean heat transport in that the eddy transport opposes the wind-driven mean transport (Fig.3.4a). In the Deep Tropics, contrary to the Southern Ocean, it is a poleward mean transport that dominates the total whereas the eddy transport is oriented equatorward. Another difference is that it is barotropic and not baroclinic instability that generates the eddy transport. Indeed, Tropical Instability Waves are clearly visible in instantaneous SST maps (Fig.4.3). They are larger than mesoscale eddies ($L \sim 1000km$) because of the low Coriolis parameter. They are fed by the strong meridional shear of zonal Equatorial currents (see next section). It can be shown using the Transformed Eulerian Mean formalism, similarly as in the Southern Ocean, that because of those instabilities, the residual (mean plus eddy-driven) overturning transport, which is felt by tracers such as temperature, is much weaker

than the mean overturning due to the Tropical Cells.

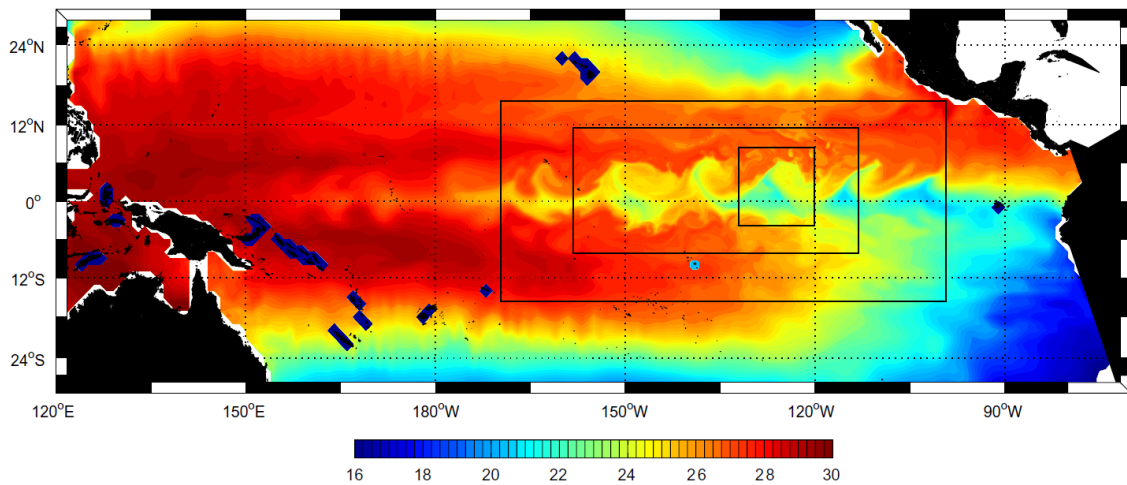


Figure 4.3: Sea surface temperature in November 1998 from a nested high-resolution simulation (36 to 4km resolution) of the Tropical Pacific (source: Marchesiello et al 2011). Tropical Instability Waves are clearly visible and they tend to reduce the meridional heat gradient and transport.

4.1.4 Tropical-subtropical connections: the Subtropical Cells

Let us zoom out for a moment and consider the meridional circulation of the wide subtropical band ($\pm 30^\circ$ of latitude). We have seen that across this region, there is poleward Ekman transport driven by Easterly winds. Although it varies with latitude, in a meridionally integral sense, it corresponds to the upper branch of a planetary overturning cell that upwells in the Equator where northward Ekman transports are accelerated and sinks within the subtropical gyre where they cancel out (Fig.4.2a). Once again, by continuity, a return flow must exist in the interior ocean. Now because of the northward interior flow within the Tropical Gyres, this southward flow occurs southwestward within the Subtropical Gyre, and then through the western boundary current of the Tropical Gyre where it feeds western equatorial basins. It ultimately upwells along the Equator. We have just described the pathway of mode waters connecting the Subtropics to the Tropics, defining the so-called Subtropical Cell (Fig.4.2b). They are the main source of interior equatorward convergence, although Tropical Cells also contribute to it (Fig.4.2b). Similarly to mode waters recirculating within the Subtropical Gyre (see Fig.2.8), they are mostly adiabatic once they subduct below the mixed layer within the Subtropical Gyre. Hence they mostly conserve their properties until they resurface at the Equator years later. Thus they might also be a source of decadal climate variability and predictability.

4.2 Zonal circulation

Although the meridional circulation drives the poleward heat transport, the most intense circulation features of the Deep Tropics are zonal. We have already mentioned the North Equatorial Current and Countercurrent, but even more intense zonal currents lie along the Equator. Their exceptional magnitude is related to the cancellation of the Coriolis acceleration at the Equator.

4.2.1 South Equatorial Currents

In the Deep Tropics, oceanic motion largely departs from Geostrophic balance. The Equatorial Rossby number is:

$$Ro = \frac{U}{fL} = \frac{U}{\beta L^2} \simeq \frac{R_a U}{2\Omega y^2} \simeq \frac{1 \times 10^7}{1.5 \times 10^{-4} \times (2.5 \times 10^5)^2} \simeq 1$$

with $y = 250km$ (that is $\phi \simeq 2^\circ$) the meridional extent. This qualifies so-called submesoscale dynamics in the ocean. The effect of rotation is still felt by water masses, but advective effects become as important. Indeed, we also have $Ro = \zeta/f \simeq 1$. Such dynamics are usually encountered for very small oceanic scales ($\sim 1 - 10km$, see Chapter 2), but exceptionally, it also concerns large-scale motion along the Equator. The dynamical challenge is that, as we will see, all terms of the horizontal momentum equations seen in Chapter 2 become important (Fig.4.5). However, outside of the Deep Tropics, the dynamics rapidly become quasi-geostrophic again. Indeed, the Rossby radius scales as $1/y^2$, so that $Ro \sim 0.1$ for $y \simeq 250km \times \sqrt{10} \simeq 800km$, that is at $\phi \simeq 7^\circ$ of latitude. Both dynamical regimes characterize the South Equatorial Currents which confusingly gather westward currents extending from $3^\circ N$ to $20^\circ S$.

Along the Equator, the Coriolis acceleration can no longer balance the westward wind stress caused by Easterlies. Hence the flow is accelerated westwards until water masses that accumulate in the western Warm Pool build up an eastward pressure gradient that balances wind stress. We have just characterized the Equatorial South Equatorial Current (eSEC, Fig.4.4). Its pressure gradient is clearly visible at surface from the zonal slope of the dynamic sea level, as identified in Chapter 1, Fig.2.1. The abyssal ocean being mostly at rest, this means from Margules's relation seen in Chapter 1 that an opposite thermocline slope exists in the interior ocean (Fig.4.6a-b). With a typical dynamic sea level difference of $\Delta\eta \simeq -60cm$ in the Equatorial Pacific, Margules's relation gives a thermocline depth difference of $\Delta h \simeq -200 \times \Delta\eta \simeq +120m$. Such a zonal section is typical in the tropical Pacific of a neutral ENSO anomaly (Fig.4.6c), and it is enhanced during La Niña events.

Exercise: zonal sea level slope within the frictional surface layer. We suppose a surface frictional layer of depth $H = 100m$ where zonal pressure gradients balance the surface wind stress. We assume a homogeneous layer of density $\rho_0 = 1025kg/m^3$. Deduce the zonal sea level gradient balancing a trade wind of magnitude $u_{10m} = -5m/s$. To what zonally-integrated sea level difference does it correspond in the Equatorial Pacific of width $W = 8,000km$? We assume $g \sim 10m^2/s$, $\rho_a \sim 1kg/m^3$ and $C_d \sim 2 \times 10^{-3}$.

Solution: the zonal momentum equation writes as:

$$\begin{aligned} 0 &= -\frac{1}{\rho_0} \frac{\partial P}{\partial x} + \frac{\partial}{\partial z} \left(\kappa_{zu} \frac{\partial u}{\partial z} \right) \\ \iff 0 &= -g \frac{\partial \eta}{\partial x} + \frac{\partial}{\partial z} \left(\kappa_{zu} \frac{\partial u}{\partial z} \right) \end{aligned}$$

Integrating over the frictional surface layer yields:

$$\begin{aligned} gH \frac{\partial \eta}{\partial x} &= \left[\kappa_{zu} \frac{\partial u}{\partial z} \right]_{-H}^{\eta} \\ &= \frac{\tau_x}{\rho_0} = -\frac{\rho_a C_d u_{10m}^2}{\rho_0} \\ \implies \Delta\eta &= -\frac{W \rho_a C_d u_{10m}^2}{\rho_0 g H} \simeq -40cm \end{aligned}$$

which is of the right order of magnitude.

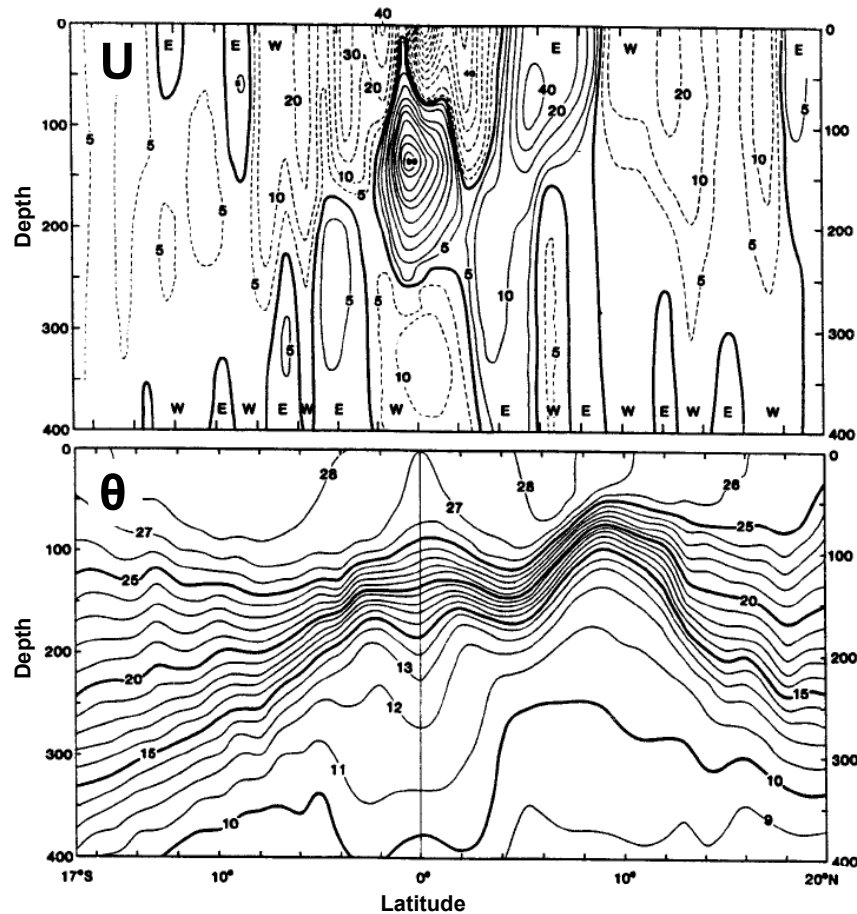


Figure 4.4: Observed meridional section of zonal currents and potential temperature across the central Tropical Pacific (155°W , between Tahiti and Hawaii, source: Lu et al 1998). At the Equator, we see the surface wind-driven eSEC and below the pressure-driven Equatorial Undercurrent. At $\sim 1 - 4^{\circ}$ of latitude, the westward nSEC and cSEC are associated with a poleward temperature gradient. Around 5° of latitude are the intense North Equatorial and the weak South Equatorial Countercurrents, associated with an equatorward temperature gradient. Finally, between $\sim 10 - 20^{\circ}$ of latitude, we find the westward North Equatorial Current and sSEC associated with a poleward temperature gradient, which are the southern branches of subtropical gyres.

On each side of the eSEC, in the Deep Tropics, lie the Northern and Central South Equatorial Currents (nSEC and cSEC, Fig.4.4). The wind stress still accelerates their westward flow, but the Coriolis acceleration becomes important so that the meridional pressure gradient also drives the westward flow. Indeed, because of the Equatorial upwelling, an intense equatorial sea level minimum causes a poleward pressure gradient and hence a westward geostrophic flow (Fig.4.4). Despite these dominant mechanisms, let us repeat that as for the eSEC, all terms of the zonal momentum equation are important in the dynamics of the nSEC and cSEC. In particular, lateral turbulent exchanges associated with Tropical Instability Waves also intervene.

Finally, outside of the Deep Tropics, the southern South Equatorial Current (sSEC, Fig.4.4) is the Southern Hemisphere counterpart of the North Equatorial Current, that is the westward return flow of the subtropical gyre. Its dynamics are quasi-geostrophic and hence simpler and not equatorial anymore.

The very large magnitude of the South Equatorial Currents located in the Deep Tropics (\sim

1m/s, Fig.4.4) reveals the weakness of Coriolis acceleration. First, because surface currents are more aligned to surface winds, the wind work is largely increased which permits higher levels of kinetic energy, despite modest winds along the Equator. Second, the vertical extent of the wind-driven current is not limited anymore by Coriolis acceleration, so that it can reach much higher depth ($h \sim 200m$) than Ekman currents ($h_E \sim 50m$). Indeed, vertical turbulent momentum fluxes are not balanced anymore by Coriolis acceleration, so that they must penetrate deeper for other terms of the zonal momentum equation (e.g. pressure gradient force, lateral turbulent fluxes, interactions with the Equatorial Undercurrent, see Fig.4.5) to balance them.

4.2.2 North Equatorial Countercurrent

Although it also constitutes the southern edge of the Northern Tropical Gyre, the North Equatorial Countercurrent's very large magnitude (up to $\sim 1m/s$) cannot be simply explained by gyre dynamics. Indeed, it is above all the geostrophic response to the intense Ekman suction at the northern edge of the northern Tropical Cell. The meridional pressure gradient is opposite to that along the Equator driving the nSEC and cSEC (Fig.4.4), so that geostrophic currents are eastward. We note that the mechanism resembles the Antarctic Circumpolar Current responding to Ekman suction to the north of the Deacon Cell. However in this case, the magnitude of zonal currents is more due to the weak Coriolis parameter than to the large meridional pressure gradient. Indeed, similarly to Ekman currents within the Tropical Cells, the Coriolis parameter is weak at its latitude ($\sim 5^\circ$) so that intense geostrophic currents are required for the geostrophic balance to be reached. Also, a striking difference is that the North Equatorial Countercurrent opposes the surface wind stress, contrary to the Antarctic Circumpolar Current. The relative weakness of Coriolis acceleration also means that other terms of the horizontal momentum balance matter for the dynamics of the North Equatorial Countercurrent. Note that due to the meridional asymmetry of the overlying atmosphere, a South Equatorial Countercurrent is weak to absent in the Southern Hemisphere.

4.2.3 Equatorial undercurrent

The Equatorial Undercurrent is probably the most striking illustration of the unique nature of Equatorial dynamics. This depth-intensified current reaches a maximum of $\sim 1m/s$ around 100 – 200m depth with no surface signature (Fig.4.4 and Fig.4.6c). It constitutes the strongest oceanic current that is not surface-intensified, and it is associated with the largest vertical and lateral shears of the World ocean. It is centered at the Equator, so that its direction is opposite to the local wind forcing. Its meridional shear causes strong barotropic instabilities that generate the Tropical Instability Waves, themselves crucial to its equilibration (Fig.4.5). More generally, every single term of the zonal momentum equation is important for its dynamics and no approximation can be made (Fig.4.5).

From a zonal point of view the Equatorial Undercurrent can be separated into a western acceleration and an eastern deceleration sector (Fig.4.5). To the west, the zonal pressure gradient generated by surface South Equatorial currents is not equilibrated anymore by frictional stresses below the frictional layer of depth $H \simeq 100m$. Hence an intense zonal acceleration of the flow occurs. Assuming the zonal pressure gradient is purely barotropic (namely, driven by the sea level gradient), the zonal momentum equation writes as:

$$\frac{du}{dt} = -g \frac{\partial \eta}{\partial x} \simeq +10 \times \frac{0.60}{8 \times 10^6} \simeq 10^{-6} m/s^2$$

with $\frac{du}{dt} \simeq u \frac{\partial u}{\partial y}$ for a purely zonal steady state. Thus integrating from the western boundary where

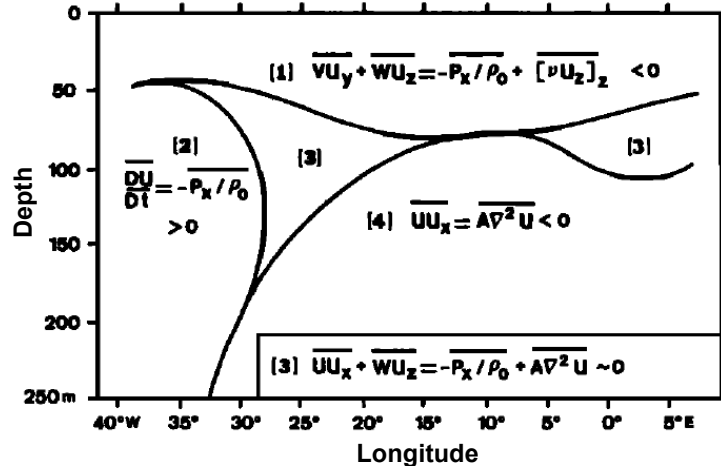


Figure 4.5: Zonal momentum balance along the Equatorial Atlantic from a numerical model (source : Wacongne 1989). All terms of the momentum balance are important. Three sectors clearly stand out: the surface eSEC area (1) under the effect of wind stress, the western Equatorial Undercurrent (2) accelerated by the pressure gradient and the eastern Equatorial Undercurrent (4) slowed down by meridional eddy export of momentum. In between are transitional areas (3) involving all terms except vertical friction.

the boundary condition imposes no normal flow, we obtain:

$$u(t) = 10^{-6}t; x(t) = 0.5 \times 10^{-6}t^2$$

$$\Rightarrow u = 1.5m/s \iff t = 1.5/10^{-6} \simeq 15 \text{ days}; x = 0.5 \times 10^{-6} \times 1.5^2 \times 10^{12} \simeq 1,000km$$

This gives a lower bound for the western boundary width where the Equatorial undercurrent is accelerated. To the East, the zonal pressure gradients weaken and meridional eddy momentum fluxes due to the Tropical Instability Waves are a sink of zonal momentum. Also, due to the intense equatorial upwelling, the Equatorial Undercurrent is slanted. It is shallower to the East, where it can ultimately feel surface wind stress that slows it down. In this case, the zonal momentum equation writes as:

$$\frac{du}{dt} = -g \frac{\partial \eta}{\partial x} + \frac{\partial}{\partial z} (\kappa_{zu} \frac{\partial u}{\partial z}) + \frac{\partial}{\partial y} (\kappa_{hu} \frac{\partial u}{\partial y})$$

The second term to the right hand side is the vertical turbulent momentum flux that transmits downward the wind stress and is opposed to the Equatorial undercurrent. The third term is the eddy meridional momentum flux. It is negative because within the Equatorial Undercurrent, the meridional curvature of velocities is negative (barotropic instability exports momentum poleward).

However, from a meridional point of view, the picture is slightly different. Indeed, as we have seen regarding the meridional transport, water masses that feed the Equatorial Undercurrent come partly from the Deep Tropics, and mostly from the Subtropics. Those water masses are essentially adiabatic, so that their potential vorticity is reasonably conserved. For an isopycnal layer of thickness h , it writes as $(f + \zeta)/h$. Assuming that the water parcel has subducted at a latitude y_S where $\zeta_S \ll f_S$, that is $Ro \ll 1$, then we deduce by conservation of potential vorticity:

$$\frac{\zeta + \beta y}{h} = \frac{f_S}{h_S} = \frac{\beta y_S}{h_S}$$

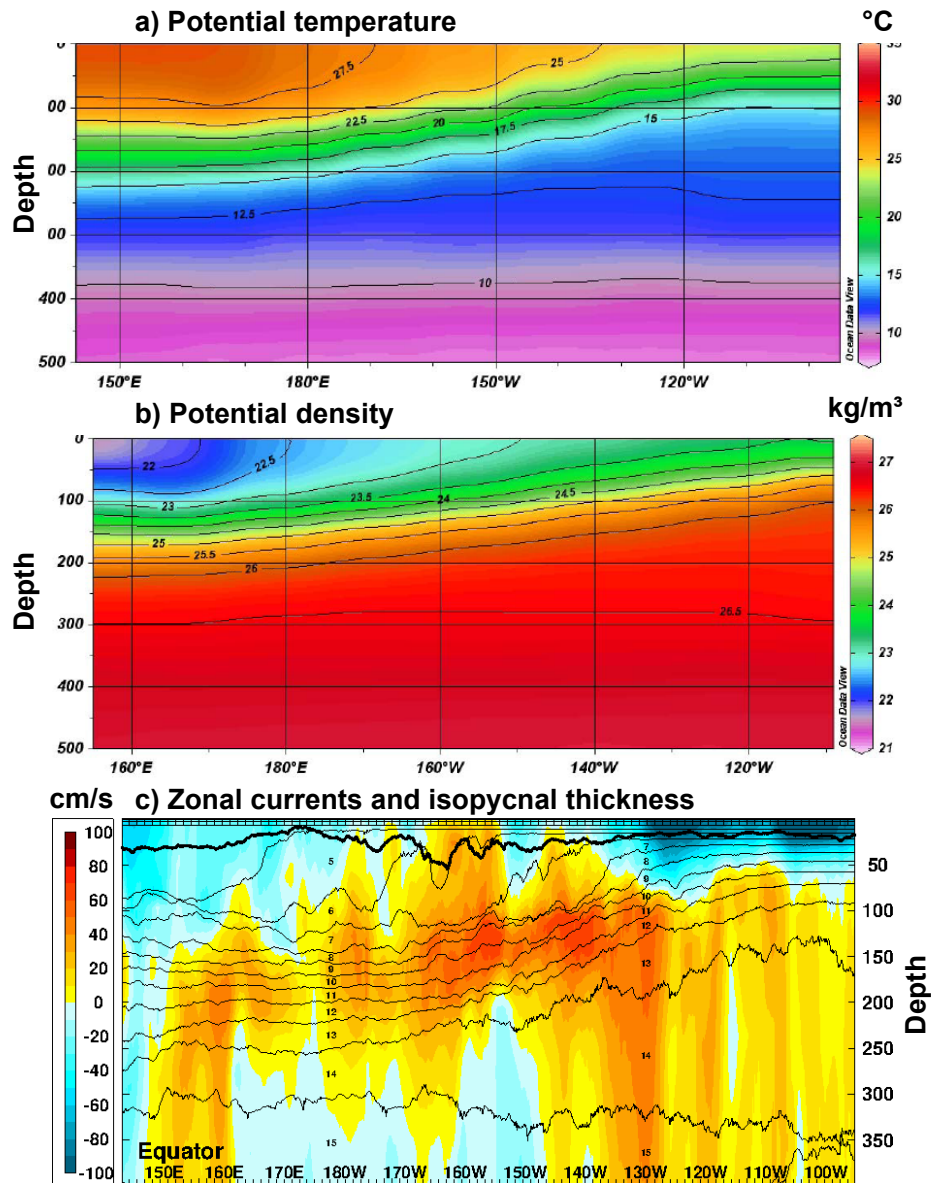


Figure 4.6: Observed mean zonal section of a) potential temperature and b) potential density along the Equatorial Pacific (source: Leif Thomas's lecture) and c) near real-time zonal current and isopycnal thickness (layers numbered with increasing density) in September 2018 from MYCOM analysis (source: US Navy). A clear zonal temperature and hence potential density gradient is visible, which illustrates the westward eSEC and equatorial upwelling. It induces the intense Equatorial Undercurrent which follows isopycnals and is progressively upwelled along its path. The ENSO anomaly is here near neutral.

If we assume zonal currents dominate ($\zeta \simeq -\frac{\partial u}{\partial y}$), we deduce an upper bound for zonal velocities at the Equator assuming the isopycnal thickness remains constant $h = h_S$ and the parcels subduct

with a weak velocity $u(y_S) \simeq 0$:

$$\begin{aligned} \frac{\partial u}{\partial y} &= \beta(y - y_S) \\ \implies u(y = 0) &= \beta y_S^2 / 2 - u(y_S) \simeq \beta y_S^2 / 2 \\ \implies u(y = 0) &= 1 \text{ m/s} \iff y_S \simeq 400 \text{ km} \end{aligned}$$

From an Eulerian point of view, this gain of zonal momentum at the Equator comes from the meridional acceleration of geostrophic currents, which drives a meridional convergence of zonal momentum: $-v \frac{\partial u}{\partial y} > 0$ (Fig.4.5). However, water masses that converge to the Equator are mostly subtropical waters from $\sim 20 - 30^\circ$ of latitude, and not from the Tropical Cells as suggested from the result above. Indeed, water columns are also squashed when moving equatorward to conserve their potential vorticity, which is evident from the shoaling of isopycnals towards the Equator (Fig.4.4). Hence the role of meridional convergence is in reality more secondary than suggested when assuming a constant isopycnal thickness.

Exercise: what would happen to the tropical Pacific circulation if the Equatorial trades were suddenly reversed into Westerlies?

Response: El Niño. Namely: a reversal of the eSEC and of the Tropical Gyres, hence also of the nSEC, cSEC, a cancellation of the Tropical Gyre circulation and of the North Equatorial Countercurrent. The consequence for temperature distributions: weakening to cancellation of the zonal sea level, temperature and hence pressure gradients, and as a consequence also weakening of the Equatorial Undercurrent. This response is not instantaneous and involves mostly Equatorial Kelvin and Rossby waves of typical propagation times ~ 2 months and ~ 6 months across the Tropical Pacific. Note that mid-latitude Rossby waves take typically decades to cross oceanic basins: this is why the Equatorial ocean variability is coupled to the atmosphere, contrary to mid-latitudes.